© 2018. Published by The Company of Biologists Ltd | Journal of Cell Science (2018) 131, jcs219527. doi:10.1242/jcs.219527

RESEARCH ARTICLE

Cullin-3–KCTD10-mediated CEP97 degradation promotes primary cilium formation

Tomoaki Nagai[1,*], Sachiho Mukoyama[1,*], Harumi Kagiwada[2], Naoki Goshima[2] and Kensaku Mizuno[1,‡]

ABSTRACT

Primary cilia are antenna-like sensory organelles that transmit various extracellular signals. Ciliogenesis requires the removal of CP110 and its interactor CEP97 from the mother centriole for initiating ciliary axoneme extension, but the underlying mechanism remains unknown. Here we show that, upon serum starvation, CEP97 is partially degraded by the ubiquitin-proteasome system. CEP97 was polyubiquitylated in serum-starved cells, and overexpression of a non-ubiquitylatable CEP97 mutant effectively blocked CP110 removal and ciliogenesis induced by serum-starvation. Through several screening steps, we identified the cullin-3–RBX1–KCTD10 complex as the E3 ligase that mediates CEP97 degradation and removal from the mother centriole. Depletion of each component of this E3 complex caused aberrant accumulation of CEP97 on the centrosome, suppressed the removal of CEP97 and CP110 from the mother centriole, and impaired ciliogenesis. Moreover, KCTD10 was specifically localized to the mother centriole. These results suggest that CEP97 degradation by the cullin-3–RBX1–KCTD10 complex plays a crucial role in serum-starvation-induced CP110 removal and ciliogenesis.

KEY WORDS: Primary cilia, CEP97, CP110, Cullin-3, KCTD10, Ubiquitylation

INTRODUCTION

Primary cilia are non-motile cilia protruding from the plasma membrane of the majority of vertebrate cells. They function as cellular antennae that sense and transmit chemical and mechanical signals from the extracellular milieu and, thereby, play essential roles in tissue development and homeostasis (Basten and Giles, 2013; Gerdes et al., 2009; Goetz and Anderson, 2010). Deficits in the formation of primary cilia cause various human disorders that are collectively termed ciliopathies, including polycystic kidney disease, retinal degeneration, visceral inversion, polydactyly and neurodegeneration (Fliegauf et al., 2007).

Primary cilia are generated by the extension of a microtubule-based axoneme from the basal body, which is derived from the mother centriole, the older of the two centrioles in the centrosome (Basten and Giles, 2013; Gerdes et al., 2009; Goetz and Anderson, 2010). Whereas extensive studies have identified a large number of molecules that participate in primary cilium formation, the molecular mechanisms of ciliogenesis still remain elusive. In cultured mammalian cells, ciliogenesis is triggered by serum starvation, indicating that ciliogenesis is tightly correlated with exit from the cell cycle (Izawa et al., 2015; Nigg and Raff, 2009; Sánchez and Dynlacht, 2016). The centrosomal protein CP110, which localizes on the distal ends of both mother and daughter centrioles, forms a cap to block the elongation of axonemal microtubules and, thereby, prevents inappropriate ciliogenesis in proliferating cells (Bettencourt-Dias and Carvalho-Santos, 2008; Kobayashi and Dynlacht, 2011; Sánchez and Dynlacht, 2016; Tsang and Dynlacht, 2013). In response to cell cycle exit signals, CP110 is removed selectively from the mother centriole, which is an essential step for the quiescence-induced ciliogenesis (Bettencourt-Dias and Carvalho-Santos, 2008; Kobayashi and Dynlacht, 2011; Sánchez and Dynlacht, 2016; Tsang and Dynlacht, 2013). Previous studies demonstrated that TTBK2, MARK4 and Centrin2 are required for this step (Goetz et al., 2012; Kuhns et al., 2013; Prosser and Morrison, 2015), and some miRNAs affect ciliogenesis by controlling expression levels of CP110 (Cao et al., 2012; Song et al., 2014). However, how these molecules regulate the removal of CP110 from the mother centriole at the early step of ciliogenesis is largely unknown.

CEP97 interacts and cooperates with CP110 to suppress primary cilium formation (Spektor et al., 2007). Depletion of CEP97 decreases CP110 protein level and suppresses CP110 localization to the centrioles, suggesting that CEP97 is crucial for regulating the stability and centriolar recruitment of CP110 (Spektor et al., 2007). Similar to CP110, CEP97 is specifically removed from the mother centriole in quiescent cells. However, the mechanisms of CEP97 removal from the mother centriole and its roles in CP110 removal and ciliogenesis have remained unknown.

The ubiquitin-proteasome system is a protein degradation system that regulates many cellular and physiological processes (Hershko and Ciechanover, 1998). Previous studies have shown that E3 ubiquitin ligases, such as pVHL, CRL3-KCTD17 and MIB1, promote or suppress ciliogenesis through the ubiquitylation and degradation of negative or positive regulators of ciliogenesis (Kasahara et al., 2014; Thoma et al., 2007; Villumsen et al., 2013; Wang et al., 2016). CP110 was reported to be ubiquitylated and degraded by the E3 ligase $SCF^{cyclinF}$ during G2 and M phases (D'Angiolella et al., 2010). Recent studies also showed that NEURL-4 and EDD-DYRK2-$DDB1^{VprBP}$, the components of E3 ligases, are involved in ciliogenesis through CP110 ubiquitylation (Hossain et al., 2017; Loukil et al., 2017). However, the precise mechanism of the removal of CP110 and CEP97 during the early stage of ciliogenesis is still unknown.

In this study, we explore the mechanism of CEP97 degradation and its roles in CP110 removal and ciliogenesis induced by serum-starvation. We show that the ubiquitin-proteasome system controls serum-starvation-induced CEP97 degradation. We provide evidence that the cullin-3 (CUL3)–RBX1–KCTD10 complex acts

[1]Department of Molecular and Chemical Life Sciences, Graduate School of Life Sciences, Tohoku University, Sendai, Miyagi 980-8578, Japan. [2]Functional Proteomics Team, Molecular Profiling Research Center for Drug Discovery, National Institute of Advanced Industrial Science and Technology, Tokyo 135-0064, Japan. *These authors contributed equally to this work

‡Author for correspondence (kmizuno@biology.tohoku.ac.jp)

K.M., 0000-0001-9386-4294

Received 25 April 2018; Accepted 19 October 2018

Journal of Cell Science (2018) 131, jcs219527. doi:10.1242/jcs.219527

as the E3 ligase that mediates serum-starvation-induced CEP97 degradation, leading to CP110 removal and ciliogenesis.

RESULTS

CEP97 is degraded upon serum starvation by the ubiquitin-proteasome system

CEP97 and CP110 cooperatively suppress cilium formation, and the removal of these proteins from the mother centriole is required for serum-starvation-induced ciliogenesis (Spektor et al., 2007). We examined the effects of CEP97 knockdown on the protein level and centriolar localization of CP110 in human telomerase-immortalized retinal pigmented epithelial 1 (RPE1) cells. As reported (Spektor et al., 2007), knockdown of CEP97 decreased CP110 protein level (Fig. 1A) and suppressed centriolar localization of CP110 (Fig. S1A), suggesting that CEP97 plays a crucial role in supporting the stability and centriolar recruitment of CP110. In contrast, knockdown of CP110 did not affect CEP97 protein level (Fig. 1A).

A previous study has shown that the CEP97 protein level was reduced in serum-starved cells (Spektor et al., 2007). We also observed that the Cep97 protein level decreased after serum starvation in RPE1 cells (Fig. 1B). CEP97 did not completely disappear in serum-starved cells, which probably reflects its retention at the daughter centriole even after serum starvation (Fig. 1C, left). To examine the mechanism of the decrease in CEP97 protein level, RPE1 cells were serum-starved for 24 h and treated with the proteasome inhibitor MG-132. This treatment blocked the serum-starvation-induced decrease in CEP97 protein level (Fig. 1B), suggesting that CEP97 is degraded upon serum starvation by the ubiquitin-proteasome system.

In serum-starved cells, CEP97 is removed from the mother centriole and remains present only on the daughter centriole (Spektor et al., 2007). We next examined the effect of MG-132 treatment on CEP97 localization in serum-starved RPE1 cells. Immunostaining with anti-CEP97 antibody revealed that CEP97 was localized to only one centriole in serum-starved control cells, whereas MG-132 treatment caused a marked accumulation of CEP97 on two centrioles and several dots near the centrosome (Fig. 1C,D). Treatment with small interfering RNA (siRNA) targeting *CEP97* abolished CEP97 immunofluorescence signals in MG-132-treated cells (Fig. S1B), indicating that the Cep97 immunostaining signal was specific. MG-132 treatment did not increase the number of cells with >2 centrioles (as measured by centrin and γ-tubulin immunostaining) in serum-starved RPE1 cells (Fig. S1C,D), indicating that MG-132-induced CEP97 accumulation near the centrosome did not result from centriole amplification. In addition, we examined the effect of MG-132 on serum-starvation-induced cell quiescence by immunostaining for Ki-67, a commonly used marker for proliferating cells. In the control experiments, the number of Ki-67-positive cells was decreased upon serum starvation and increased after serum had been added again (Fig. S1E,F). MG-132 treatment did not increase the number of Ki-67-positive cells under serum-starved conditions (Fig. S1G,H), indicating that MG-132 treatment had no effect on serum starvation-induced cell quiescence under our experimental conditions.

To examine whether CEP97 is ubiquitylated in cultured cells, HEK293T cells were co-transfected with YFP-tagged CEP97 and HA-ubiquitin, and cultured in the presence or absence of MG-132. The cell lysates were then analyzed by immunoprecipitation with an anti-GFP nanobody, followed by immunoblotting with an anti-HA antibody. Polyubiquitylation of YFP-CEP97 was observed predominantly after the treatment with MG-132 (Fig. 1E). We also demonstrated that endogenous CEP97 was more prominently polyubiquitylated in MG-132-treated RPE1 cells under serum-starved quiescent conditions than in the same cells during S phase arrest (Fig. 1F). These results suggest that CEP97 was preferentially degraded upon serum starvation by the ubiquitin-proteasome system.

A non-ubiquitylatable CEP97 mutant effectively suppresses CP110 removal and ciliogenesis

To investigate the role of CEP97 ubiquitylation in ciliogenesis, we constructed a non-ubiquitylatable mutant of CEP97 and analyzed the effect of its overexpression on ciliogenesis. A proteomic database of post-translational modifications predicted K582 and K618 as the ubiquitylated residues of CEP97 (Mertins et al., 2013). We, therefore, constructed the CEP97(3KR) mutant, in which K582, K618 and K617 were replaced by arginine residues (Fig. 2A). Ubiquitylation assays revealed that the level of ubiquitylation of CEP97(3KR) was reduced in MG-132-treated cultured cells, compared with that of wild-type (WT) CEP97 (Fig. 2B). It has been reported that overexpression of CEP97(WT) suppresses serum-starvation-induced ciliogenesis, but its suppressive effect is limited (Spektor et al., 2007), possibly because CEP97(WT) is unstable due to ubiquitylation and proteasomal degradation under serum-starved conditions. To test this assumption, we compared the effect of overexpression of non-ubiquitylatable CEP97(3KR) with that of CEP97(WT) on serum-starvation-induced ciliogenesis. RPE1 cells transfected with YFP-tagged CEP97(WT) or CEP97(3KR) were serum-starved and then immunostained with antibodies against Arl13b (as a marker of ciliary membranes) and FGFR1 oncogene partner (FOP; as a marker of mother and daughter centrioles; Lee and Stearns, 2013) (Fig. 2C). CEP97(WT)-YFP and CEP97(3KR)-YFP were enriched on two centrioles in non-ciliated cells (Fig. 2C). Whereas primary cilia were formed in 63% of control YFP-expressing cells, overexpression of CEP97(WT) only modestly reduced the fraction of ciliated cells to 44%. Notably, overexpression of CEP97(3KR) reduced the fraction of ciliated cells more severely to 27% (Fig. 2D). These results suggest that CEP97 ubiquitylation is crucial for serum-starvation-induced ciliogenesis.

Both CEP97 and CP110 are removed from the mother centriole upon serum starvation but remain localized to the daughter centriole in ciliated cells (Spektor et al., 2007). We next examined the effects of overexpressing CEP97(WT) or CEP97(3KR) on CP110 removal from the mother centriole after serum starvation. RPE1 cells were transfected with YFP-tagged CEP97(WT or 3KR), serum-starved, and stained with antibodies against CP110, FOP and CEP170 (as a marker of the mother centriole; Guarguaglini et al., 2005) (Fig. 2E). In most control YFP-expressing cells, CP110 was localized to a CEP170-negative single centriole, indicating that CP110 had been removed from the mother centriole. Overexpression of CEP97(WT) or CEP97(3KR) decreased the population of cells with CP110 localized to a CEP170-negative single centriole and inversely increased the population of cells with CP110 localized to two centrioles (Fig. 2E). Quantitative analyses showed that the population of cells with CP110 localized to one centriole was 66% in control YFP-expressing cells, but it was decreased to 45% and 30% by overexpression of CEP97(WT) and CEP97(3KR), respectively (Fig. 2F). These results suggest that the non-ubiquitylatable CEP97 variant more severely suppresses the removal of CP110 from the mother centriole and that CEP97

Journal of Cell Science (2018) 131, jcs219527. doi:10.1242/jcs.219527

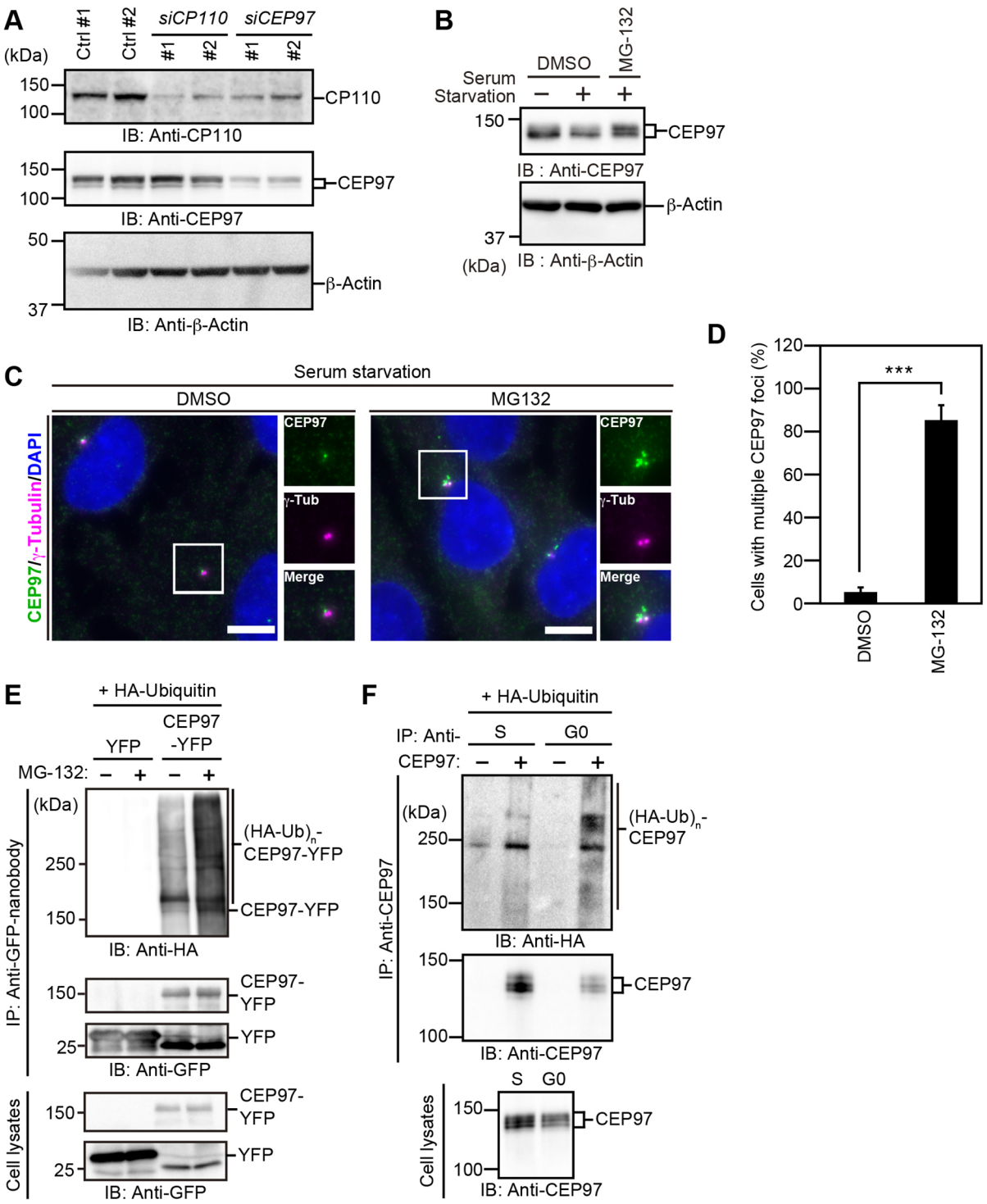

Fig. 1. CEP97 is degraded upon serum starvation by the ubiquitin-proteasome system. (A) Effects of CP110 or CEP97 knockdown on the expression of each protein. RPE1 cells were transfected with corresponding siRNAs, and cell lysates were analyzed by immunoblotting (IB) with anti-CEP97, anti-CP110 and anti-β-actin antibodies. (B) Changes in the levels of CEP97 upon serum starvation and effect of MG-132 treatment. RPE1 cells were serum starved for 24 h and then treated with DMSO or 0.3 µM MG-132 in the medium containing 0.2% FCS for 24 h. Cell lysates were analyzed by IB with anti-CEP97 and anti-β-actin antibodies. (C) MG-132 induces aberrant accumulation of CEP97 on and near the centrosome. RPE1 cells were treated as in B. Cells were fixed and stained with anti-CEP97 (green) and anti-γ-tubulin (magenta) antibodies. DNA was stained with DAPI (blue). Right panels show magnified images of the white boxes. Scale bars: 10 µm. (D) Quantification of the percentage of cells with multiple CEP97 foci. Data are presented as the mean±s.e.m. from three independent experiments with >100 cells per experiment. Statistical significance was calculated using ordinary Student's *t*-test. ***P<0.001. (E) Ubiquitylation assays. HEK293T cells were co-transfected with HA-ubiquitin and YFP or CEP97-YFP. Cells were treated with DMSO or 10 µM MG-132 for 3 h and lysates were immunoprecipitated (IP) with a GST-tagged anti-GFP nanobody pre-bound to glutathione-Sepharose beads. Precipitates were analyzed by IB with anti-HA and anti-GFP antibodies. (F) Ubiquitylation assays of endogenous CEP97. RPE1 cells were transfected with HA-ubiquitin and treated with 2 mM thymidine or 0.2% FCS for 36 h to induce cell cycle arrest at S or G0 phase. Before harvesting, cells were treated with DMSO or 10 µM MG-132 for 3 h. Cell lysates were immunoprecipitated with an anti-CEP97 antibody. Immunoprecipitates were analyzed by IB with anti-HA and anti-CEP97 antibodies.

Journal of Cell Science (2018) 131, jcs219527. doi:10.1242/jcs.219527

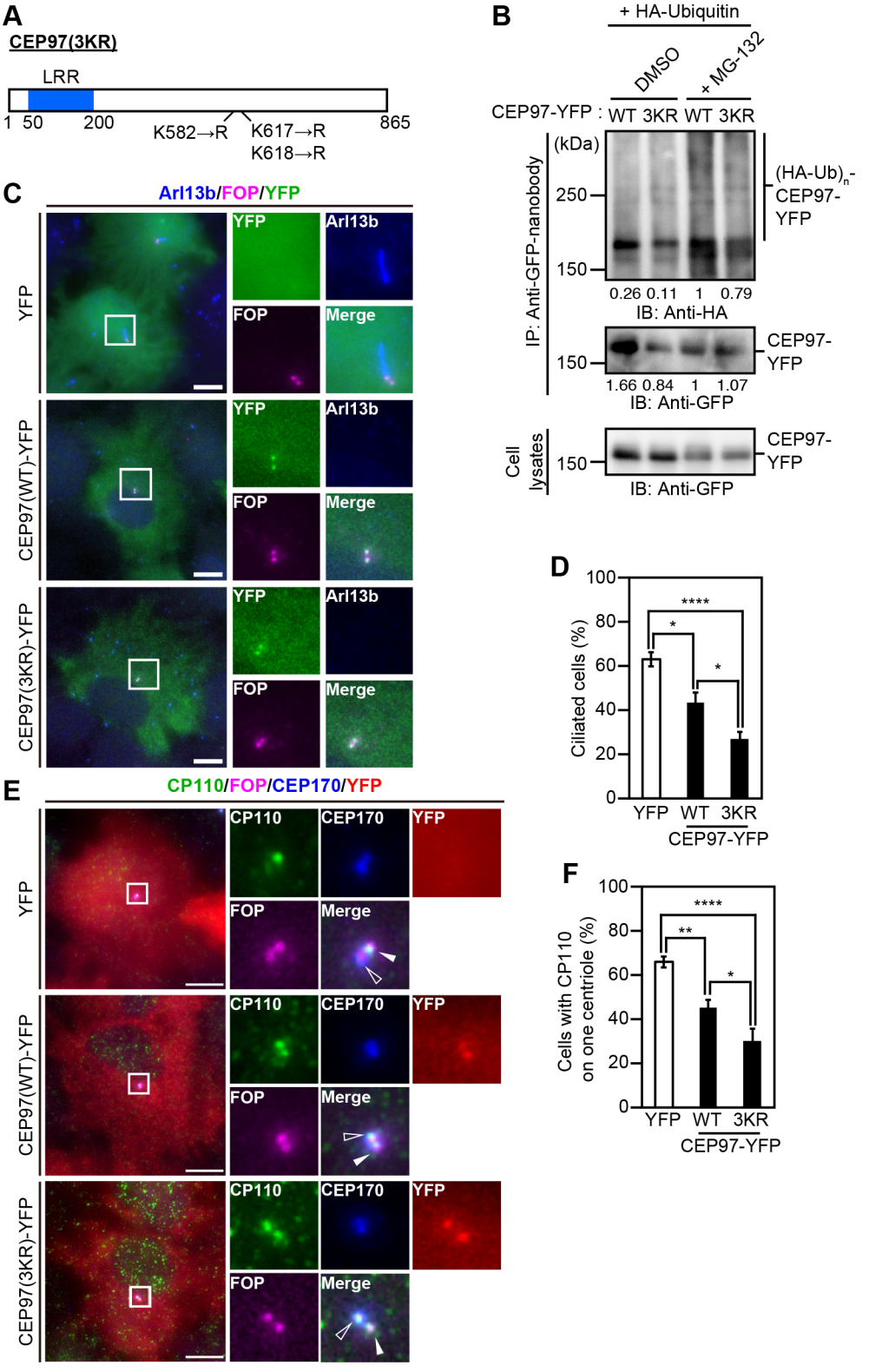

Fig. 2. Expression of a non-ubiquitylatable CEP97 mutant severely suppresses CP110 removal and ciliogenesis. (A) Schematic structure of CEP97(3KR) mutant, in which K582, K617 and K618 were replaced by arginines. LRR, leucine-rich repeat motif. Numbers indicate amino acid residues. (B) Ubiquitylation assay of CEP97(3KR). HEK293T cells were co-transfected with HA-ubiquitin and YFP-tagged CEP97(WT or 3KR). Cells were treated with DMSO or 10 µM MG-132 for 3 h. Cell lysates were precipitated with a GST-tagged anti-GFP nanobody pre-bound to glutathione-Sepharose beads, and the precipitates and lysates were analyzed by immunoblotting with anti-HA and anti-GFP antibodies. The relative intensities of immunoreactive bands are indicated under the panels. (C) Overexpression of CEP97(3KR) severely suppresses serum-starvation-induced ciliogenesis. RPE1 cells were transfected with YFP or CEP97(WT or 3KR)-YFP and serum-starved for 48 h. Cells were fixed and stained with anti-Arl13b (blue) and anti-FOP (magenta) antibodies. Cells were also imaged by YFP fluorescence (green). Scale bars: 10 µm. (D) Quantification of the percentage of ciliated cells in YFP-positive cells. Data are presented as the mean±s.e.m. from five independent experiments with >100 cells per experiment. (E) CEP97(3KR) severely suppresses serum-starvation-induced CP110 removal from the mother centriole. RPE1 cells were transfected and serum-starved as in C. Cells were fixed and stained with anti-CP110 (green), anti-FOP (magenta) and anti-CEP170 (blue) antibodies. Cells were also imaged by YFP fluorescence (red). Scale bars: 10 µm. (F) Quantification of the percentage of the cells with CP110 localized to a single centriole in YFP-positive cells. Data are presented as the mean±s.e.m. from six independent experiments with >50 cells per experiment. Right panels in C and E show magnified images of the white boxes. Outlined arrowheads in E indicate CEP170-bearing mother centrioles and white arrowheads indicate daughter centrioles. Statistical significance in D and F was calculated using ordinary one-way ANOVAs with Tukey's test. *P<0.05; **P<0.01; ****P<0.0001.

ubiquitylation plays a crucial role in serum-starvation-induced CP110 removal from the mother centriole.

CUL3 is required for CEP97 degradation and ciliogenesis

To explore the mechanism of serum-starvation-induced CEP97 ubiquitylation, we next analyzed the effects of inhibitors of E3 ubiquitin ligases on serum-starvation-induced decrease in CEP97 protein level. We used inhibitors of E3 ligases that had been shown to be involved in ciliogenesis, i.e. MLN4924, an inhibitor of cullin-RING type E3 ligases (CRLs) (Kasahara et al., 2014; Pan et al., 2004; Soucy et al., 2009); Heclin, an inhibitor of HECT-type E3 ligases (Loukil et al., 2017; Mund et al., 2014); and VH298, an

Journal of Cell Science (2018) 131, jcs219527. doi:10.1242/jcs.219527

inhibitor of pVHL (Frost et al., 2016; Thoma et al., 2007). Treatment with MLN4924 effectively blocked the decrease in CEP97 after serum starvation but treatments with Heclin or VH298 had no apparent effect on CEP97 protein levels (Fig. 3A and Fig. S2A). A previous study has shown that MG-132 treatment blocks ciliogenesis (Kasahara et al., 2014). MLN4924 also

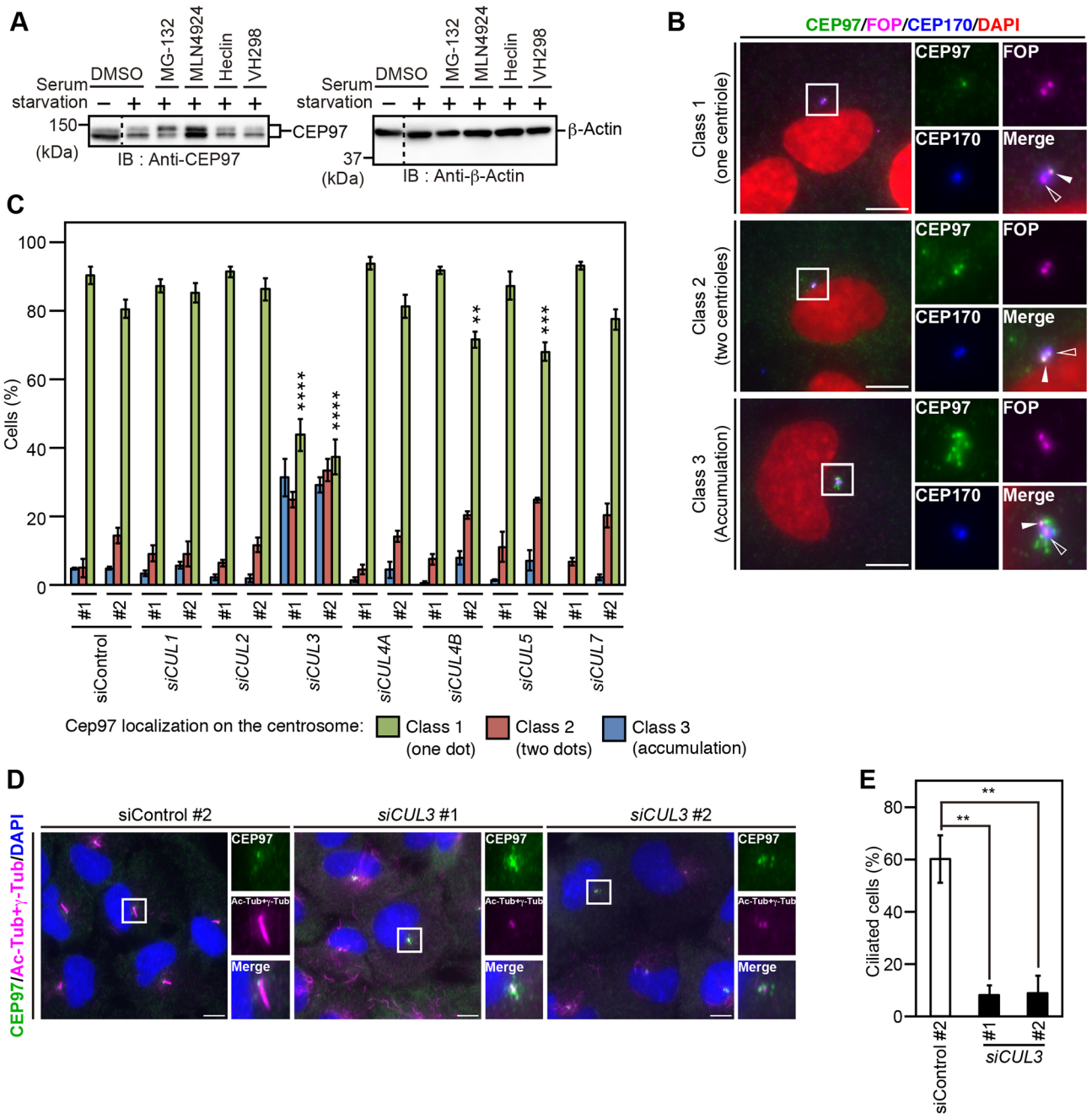

Fig. 3. Knockdown of *CUL3* causes accumulation of CEP97 on the centrosome and retention on the mother centriole, and suppresses ciliogenesis. (A) Effects of E3 ligase inhibitors on the level of CEP97 protein in serum-starved cells. RPE1 cells were serum-starved for 24 h and then treated with each inhibitor in the medium containing 0.2% FCS for 24 h. Cell lysates were analyzed by immunoblotting with anti-CEP97 and anti-β-actin antibodies. (B) Classification of cells with distinct localization and amount of CEP97 on the centrosome. RPE1 cells were transfected with control or *CUL3* siRNAs and serum-starved for 48 h. Cells were fixed and stained with anti-CEP97 (green), anti-FOP (magenta) and anti-CEP170 (blue) antibodies. DNA was stained with DAPI (red). Cells were categorized into three classes: class 1 (CEP97 localization to one centriole), class 2 (CEP97 localization to two centrioles) and class 3 (CEP97 accumulation on and around the centrosome). Scale bars: 10 µm. (C) CUL3 knockdown causes CEP97 accumulation on the centrosome and retention on the mother centriole. The percentages of cells categorized into classes 1–3 were quantified. Data are presented as the mean±s.e.m. from three independent experiments with >100 cells per experiment. (D) *CUL3* knockdown blocks ciliogenesis. RPE1 cells were transfected and serum-starved as in B. Cells were fixed and stained with anti-CEP97 (green), anti-Ac-tubulin and anti-γ-tubulin (magenta) antibodies. DNA was stained with DAPI (blue). Scale bars: 10 µm. (E) Quantification of the percentage of ciliated cells based on staining with Ac-tubulin. Data are presented as the mean±s.e.m. from three independent experiments with >100 cells per experiment. Right panels in B and D show magnified images of the white boxes. Outlined and white arrowheads in B indicate mother and daughter centrioles, respectively. Statistical significance in C and E was calculated using ordinary one-way ANOVAs with Tukey's test. ***P*<0.01; ****P*<0.001; *****P*<0.0001.

Journal of Cell Science (2018) 131, jcs219527. doi:10.1242/jcs.219527

inhibited serum-starvation-induced ciliogenesis (Fig. S2B). These results suggest that CRLs are involved in CEP97 degradation. Immunoblot analyses showed multiple anti-CEP97 immunoreactive bands. Treatment with λ-phosphatase abolished the upwards mobility shift (Fig. S2C), indicating that the upper bands are the phosphorylated forms of CEP97. Intensity levels of the upper band frequently increased after treatment with MG-132 but not with MLN4924. Thus, the relationship between CEP97 phosphorylation and degradation remains unknown.

To identify which member of the cullin family is involved in CEP97 degradation, we examined the effects of siRNA-based knockdown of each member of the cullin family (CUL1, CUL2, CUL3, CUL4A, CUL4B, CUL5 and CUL7) (Petroski and Deshaies, 2005) on the amount and localization of CEP97 to the centrosome. Transfection of cullin-targeting siRNAs effectively decreased the expression levels of each target protein in RPE1 cells (Fig. S2D). RPE1 cells were transfected with siRNAs, serum-starved, and stained with antibodies against CEP97, FOP and CEP170 (Fig. 3B). Cells were categorized into three classes according to the phenotype of CEP97 localization to the centrosome; class 1, cells with CEP97 localization to a single centriole (presumably a CEP170-negative daughter centriole); class 2, cells with CEP97 localization to two centrioles; and class 3, cells with marked accumulation of CEP97 on and near the centrosome (Fig. 3B). Quantitative analyses of the population of cells in each class revealed that most of the cells treated with control siRNAs were scored as class 1 (Fig. 3C). In contrast, treatments with two independent *CUL3*-targeting siRNAs significantly decreased the population of cells categorized into class 1, and inversely increased the population of cells categorized into class 2 and 3 (Fig. 3C). The siRNAs targeting other cullin members had only minor effects on CEP97 localization to the centrosome, compared with the effects of *CUL3*-targeting siRNAs. These results indicate that knockdown of CUL3 suppresses CEP97 degradation and removal from the mother centriole and causes its retention on the mother centriole in serum-starved cells. Additionally, immunoblot analyses showed that the level of CEP97 protein decreased upon serum starvation but CUL3 knockdown partially recovered the decrease in CEP97 protein in serum-starved cells (Fig. S3A). These results suggest that CUL3 is involved in serum-starvation-induced CEP97 degradation and its removal from the mother centriole.

We also examined the effects of knockdown of each of the cullin members on serum-starvation-induced ciliogenesis. RPE1 cells transfected with siRNAs were serum-starved and stained for CEP97, Ac-tubulin and γ-tubulin (Fig. 3D). We observed that treatments with two independent *CUL3*-targeting siRNAs significantly suppressed ciliogenesis (Fig. 3D,E). Several siRNAs targeting other cullin members also suppressed ciliogenesis but only one of each of the two siRNAs targeting *CUL1*, *CUL4A*, *CUL5* and *CUL7* suppressed ciliogenesis, probably due to their off-target effects on the gene products related to ciliogenesis, and the inhibitory effect of one of the *CUL4B*-targeting siRNAs was weaker than that of either of *CUL3*-targeting siRNAs (Fig. S3D). Together with the results shown in Fig. 3C, CUL3 is the most likely E3 ligase candidate that is involved in serum-starvation-induced CEP97 degradation and ciliogenesis.

We next examined the effect of *CUL3* knockdown on the removal of CP110 from the mother centriole. RPE1 cells transfected with *CUL3* siRNAs were serum-starved and stained with antibodies against CP110, FOP and CEP170 (Fig. 4A). Whereas most of cells transfected with control siRNA exhibited CP110 localization to one centriole (presumably a CEP170-negative daughter centriole), treatment with *CUL3* siRNAs significantly decreased the population of cells with CP110 localization to one centriole and increased the cells with CP110 localization to two centrioles (Fig. 4A,B), indicating that CUL3 is involved in the removal of CP110 from the mother centriole in serum-starved cells.

To examine whether *CUL3* knockdown affects serum-starvation-induced cell quiescence, RPE1 cells treated with *CUL3* siRNAs were serum-starved and stained for Ki-67. Knockdown of *CUL3* did not increase the population of Ki-67-positive cells (Fig. S4A,B), indicating that *CUL3* knockdown had no significant effect on serum-starvation-induced cell quiescence.

As an E3 ligase, CUL3 functions by forming a complex with broad complex/tramtrack/bric-a-brac (BTB) domain-containing proteins (adaptors that link CUL3 to substrate proteins) at the

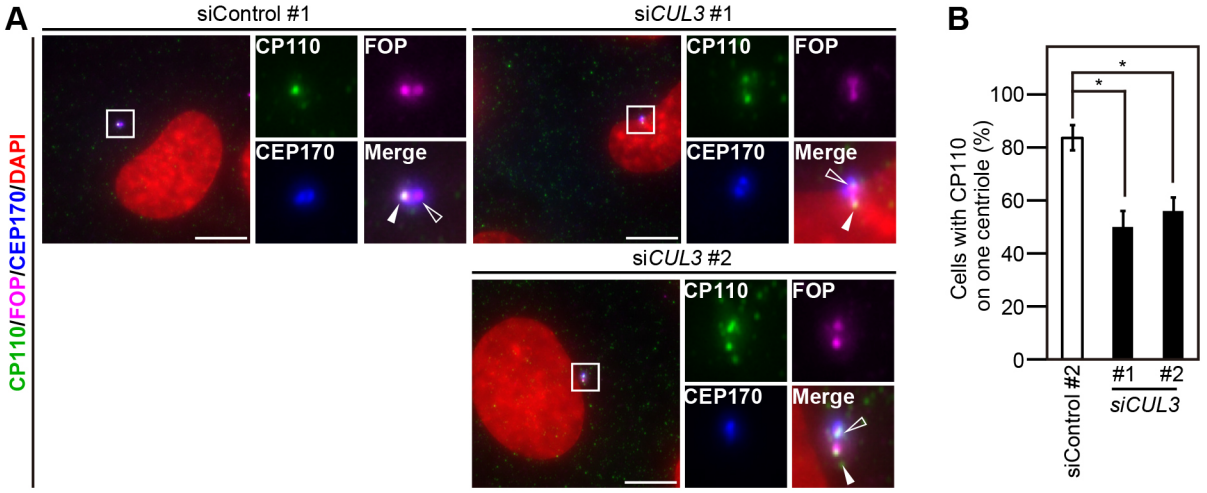

Fig. 4. Knockdown of *CUL3* suppresses the removal of CP110 from the mother centriole. (A) Immunofluorescence analyses. RPE1 cells were transfected with siRNAs targeting *CUL3* and serum-starved for 48 h. Cells were fixed and stained with anti-CP110 (green), anti-FOP (magenta) and anti-CEP170 (blue) antibodies. DNA was stained with DAPI (red). Scale bars: 10 µm. Right panels show magnified images of the white boxes. Outlined and white arrowheads indicate mother and daughter centrioles, respectively. (B) Quantitative analyses. The percentage of cells with CP110 localized to one centriole in cells treated with siRNAs targeting *CUL3*. Data are means±s.e.m. from three independent experiments with >100 cells per sample. Statistical significance was calculated using ordinary one-way ANOVAs with Tukey's test. *P<0.05.

Journal of Cell Science (2018) 131, jcs219527. doi:10.1242/jcs.219527

N-terminal region, and with RBX1 (a RING motif-containing protein that cooperatively functions with CUL1–4 for ubiquitylation of substrate proteins) at the C-terminal region (Furukawa et al., 2003; Genschik et al., 2013). To further define the role of CUL3 in CEP97 degradation, we analyzed the effect of expression of the CUL3 N-terminal fragment, CUL3(N418), which binds to the BTB proteins but not to RBX1 and, thereby, acts as a dominant-negative form of CUL3 (Cullinan et al., 2004; Furukawa et al., 2003). Overexpression of CUL3(N418) caused centrosomal accumulation of CEP97, whereas overexpression of CUL1(N452), a dominant-negative form of CUL1 (Wu et al., 2000), did not (Fig. S4G,H). Fluorescence image analyses showed that YFP-CUL3(N418), but not CUL1(N452), was enriched on the centrosome (Fig. S4G). These results further support the notion that CUL3 plays a crucial role in CEP97 degradation.

RBX1 is required for CEP97 degradation and ciliogenesis

Because RBX1 cooperatively functions with CUL3 for ubiquitylation of substrate proteins, we next examined the effect of RBX1 knockdown on the amount and localization of centrosomal CEP97 and ciliogenesis under serum-starved conditions. *RBX1*-targeting siRNAs suppressed RBX1 protein expression in RPE1 cells (Fig. S2D). Similar to the effect of *CUL3* knockdown, the treatment with two independent *RBX1*-targeting siRNAs significantly decreased the population of class 1 cells with CEP97 localization to a single centriole, and increased the population of class 2 cells with CEP97 localization to two centrioles and class 3 cells with CEP97 accumulation on the centrosome (Fig. 5A,B). Immunoblot analyses also showed that knockdown of *RBX1* partially recovered the level of CEP97 protein in serum-starved cells (Fig. S3B). These results suggest that RBX1 is involved in serum-starvation-induced CEP97 degradation and removal from the mother centriole. Similar to *CUL3* knockdown, *RBX1* knockdown significantly decreased the number of cells with CP110 localization to one centriole (Fig. 5C,D) and the number of ciliated cells (Fig. 5E,F) under serum-starved conditions. Knockdown of *RBX1* did not increase the number of Ki-67-positive cells (Fig. S4C,D). Taken together, these results suggest that the CUL3–RBX1 complex is involved in CEP97 degradation, removal of CEP97 and CP110 from the mother centriole, and ciliogenesis.

KCTD10 is required for CEP97 degradation and ciliogenesis

CUL3-mediated ubiquitylation requires BTB domain-containing proteins that serve as adaptors to link CUL3 to substrate proteins (Genschik et al., 2013). In the human genome, there are ∼180 genes encoding BTB-containing proteins (Genschik et al., 2013; Stogios et al., 2005). To identify the BTB protein(s) involved in CUL3-mediated CEP97 degradation, we first screened for the BTB proteins that have the potential to bind to CEP97 by using the visible immunoprecipitation (VIP) assay, a recently developed method to easily visualize protein-protein interactions (Fig. S5A; Katoh et al., 2015). HEK293T cells were co-transfected with CEP97-mCherry and each of Venus-tagged BTB-containing proteins. The cDNAs coding for BTB-containing proteins were obtained from a human proteome expression resource (HuPEX) cDNA library (Maruyama et al., 2012) (Table S1). We also used YFP and YFP-CP110 as negative and positive controls for CEP97-binding ability, respectively. Cell lysates were immunoprecipitated with GST-tagged anti-mCherry-nanobody and glutathione-Sepharose beads. The fluorescence of co-precipitated Venus (or YFP) on the beads bearing CEP97-mCherry was directly observed by using fluorescence microscopy. As expected, YFP fluorescence was detected on the beads for lysates of cells co-transfected with YFP-CP110, but not of those transfected with control YFP (Fig. S5B). When Venus fluorescence intensity on the beads was higher than or equal to that of YFP-CP110, we judged that this Venus-BTB protein has the potential to bind to CEP97 (Fig. S5B and Table S2). Of the 150 Venus-tagged BTB proteins examined, 24 proteins exhibited Venus fluorescence on the beads bearing CEP97-mCherry (Fig. S5B and Table S2). Reproducible results were obtained in three independent experiments.

In the second screening, we tested the effects of knockdown of individual candidates of BTB proteins on serum-starvation-induced ciliogenesis. Of the siRNAs targeting the 24 BTB proteins, both independent siRNAs targeting each of six BTB proteins significantly suppressed serum-starvation-induced ciliogenesis (Fig. S6A). As an example, the effects of *KCTD10* knockdown on ciliogenesis are shown in Fig. 6A,B. Thus, we selected these six BTB proteins as the candidates that could be involved in CEP97 degradation and ciliogenesis. We further analyzed the effect of knockdown of each of these six BTB proteins on the centrosomal localization of CEP97. Notably, among the siRNAs targeting the genes encoding those six BTB proteins, only the two independent siRNAs targeting *KCTD10* caused accumulation of CEP97 on the centrosome (Fig. 6C, Fig. S6B). Although one of the two siRNAs targeting *BTBD11* and *KCTD1* modestly increased the number of cells with CEP97 accumulation on the centrosome, their effects were weaker than those of *KCTD10*-targeting siRNAs (Fig. S6B). Knockdown efficiency of siRNAs targeting *KCTD10*, *KCTD1* and *BTBD11* was shown in Figs S2D and S6C,D. Moreover, *KCTD10* knockdown decreased the number of class 1 cells with CEP97 localization to a single centriole and increased the number of class 2 cells with CEP97 localization to two centrioles, in addition to the number of class 3 cells with CEP97 accumulation on the centrosome (Fig. 6C,D). Immunoblot analyses also showed that *KCTD10* knockdown partially recovered the level of CEP97 protein in serum-starved cells (Fig. S3C). Thus, we selected KCTD10 as the BTB protein most likely to be involved in serum-starvation-induced CEP97 degradation and ciliogenesis. Similar to knockdowns of *CUL3* and *RBX1*, knockdown of *KCTD10* significantly decreased the percentage of cells with CP110 localization to one centriole in serum-starved cells (Fig. 6E,F), indicating a crucial role of KCTD10 in the removal of CP110 from the mother centriole. Additionally, *KCTD10* knockdown did not increase the number of Ki-67-positive cells (Fig. S4E,F). These results suggest that KCTD10 is involved in degradation of CEP97, removal of CEP97 and CP110 from the mother centriole, and in ciliogenesis. The effect of *KCTD10* knockdown on CEP97 dysregulation was weaker than those of knocking down *CUL3* or *RBX1*, suggesting that other BTB components of the CUL3 E3 ligase complex are partially involved in CEP97 degradation.

To confirm the results of the VIP assay, we analyzed the interaction between CEP97 and KCTD10 by coimmunoprecipitation assays. mCherry-tagged CEP97 was coexpressed with YFP-tagged KCTD10 or control YFP in HEK293T cells and immunoprecipitated with an anti-GFP nanobody. CEP97-mCherry was effectively co-precipitated with YFP-KCTD10 but barely detectable with control YFP (Fig. 6G), indicating that KCTD10 associates with CEP97. Taken together, these results suggest that the CUL3–RBX1–KCTD10 complex is the strong candidate E3 ligase for CEP97 degradation.

Journal of Cell Science (2018) 131, jcs219527. doi:10.1242/jcs.219527

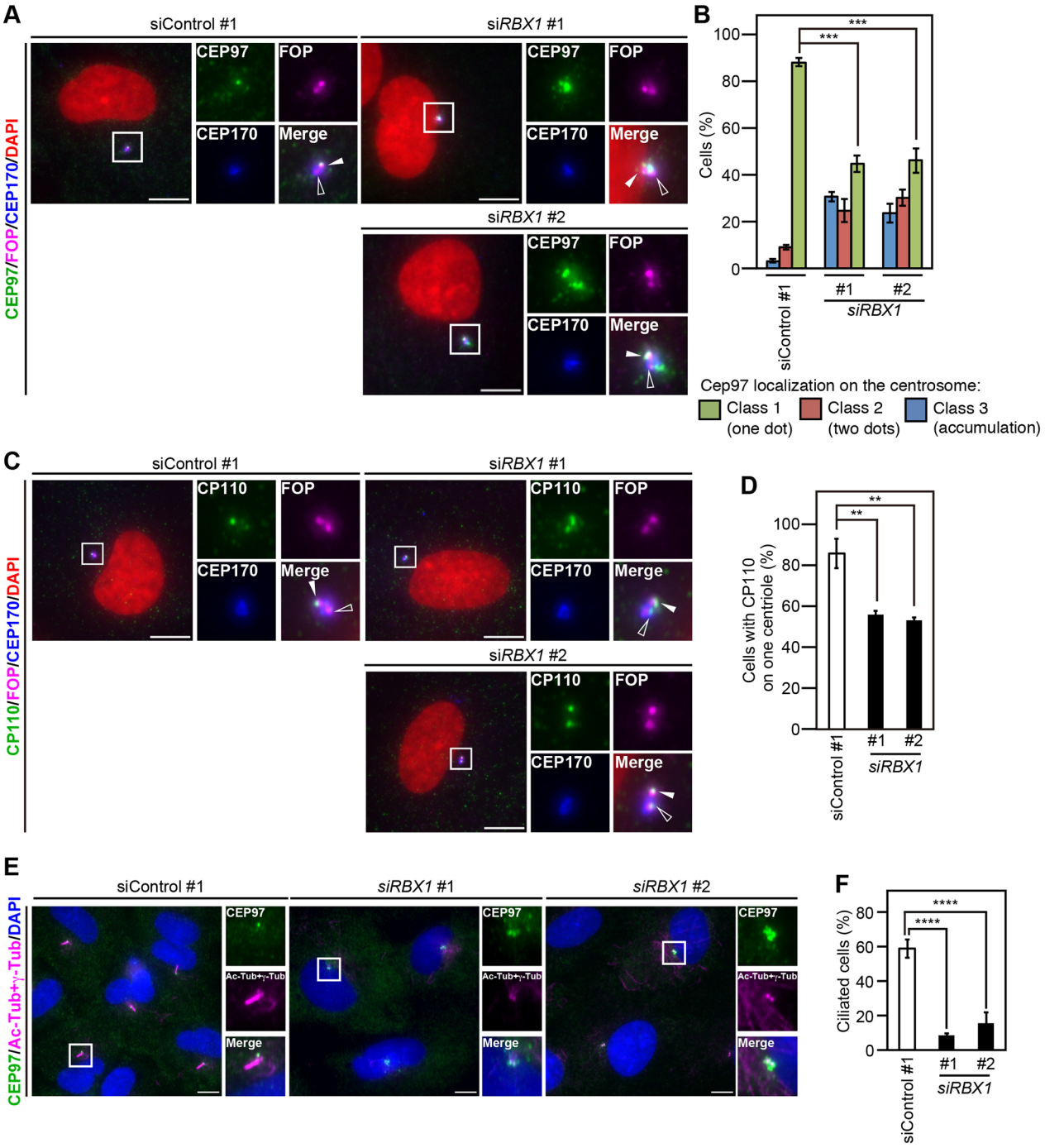

Fig. 5. RBX1 is required for CEP97 degradation, CP110 removal and ciliogenesis. (A) Knockdown of *RBX1* causes CEP97 accumulation on the centrosome and retention on the mother centriole. RPE1 cells were transfected with control or *RBX1* siRNAs and subject to serum starvation for 48 h. Cells were fixed and stained with anti-CEP97 (green), anti-FOP (magenta) and anti-CEP170 (blue) antibodies. DNA was stained with DAPI (red). (B) Quantification of the percentage of cells categorized into classes 1–3, as shown in Fig. 3C. (C) Knockdown of *RBX1* suppresses the removal of CP110 from the mother centriole. RPE1 cells were transfected with siRNAs targeting *RBX1*. Cells were treated and analyzed, as in Fig. 4A. (D) Quantitative analyses of the percentage of cells with CP110 localized to one centriole. (E) *RBX1* knockdown blocks ciliogenesis. RPE1 cells were transfected and serum-starved as in A. Cells were fixed and stained with anti-CEP97 (green), anti-Ac-tubulin and anti-γ-tubulin (magenta) antibodies. DNA was stained with DAPI (blue). (F) Quantification of the percentage of ciliated cells. Scale bars: 10 µm (A,C,E); right panels show magnified images of the white boxes. Outlined and white arrowheads indicate mother and daughter centrioles in A and B, respectively. Data are presented as the mean±s.e.m. from three, three and four independent experiments in B, D and F, respectively; with >100 cells per sample. Statistical significance was calculated using ordinary one-way ANOVAs with Tukey's test. ***P*<0.01; ****P*<0.001; *****P*<0.0001.

Expression of KCTD10 mutants impairs CEP97 degradation and ciliogenesis

BTB-containing adaptor proteins directly bind to CUL3 via the N-terminal BTB domains (Furukawa et al., 2003; Pinkas et al., 2017; Xu et al., 2003). To investigate the importance of the CUL3–KCTD10 interaction for CEP97 degradation and ciliogenesis, we constructed three KCTD10 mutants: a C-terminal fragment (C142), a BTB-domain mutant (3A) in which Ile-83, Leu-84 and Ile-85 were replaced

Journal of Cell Science (2018) 131, jcs219527. doi:10.1242/jcs.219527

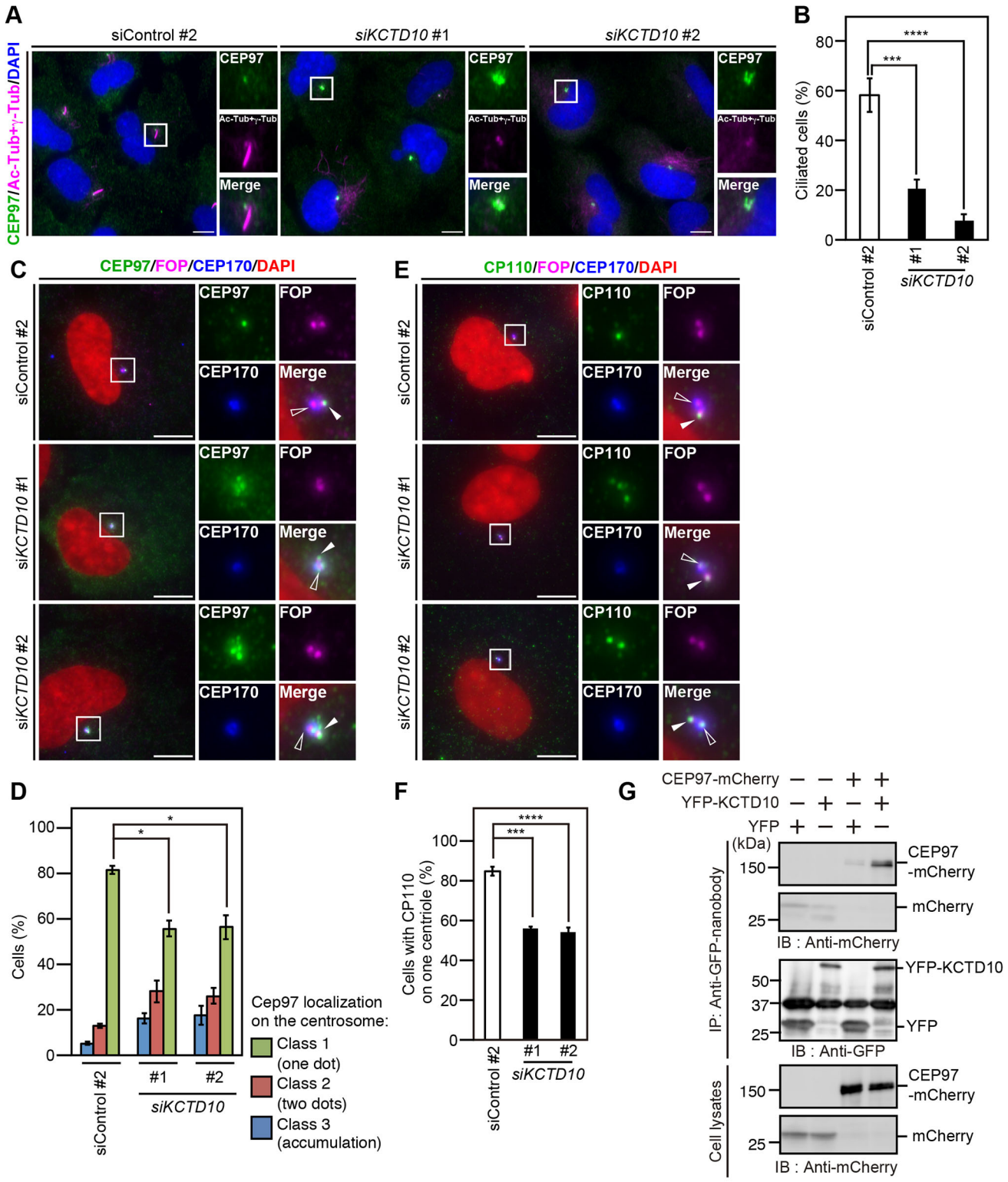

Fig. 6. See next page for legend.

by alanine residues that are known to impair CUL3-binding ability (Chen et al., 2009), and an N-terminal fragment (N145) (Fig. 7A). Co-precipitation assays revealed that CUL3 effectively co-precipitated with full-length (FL) KCTD10 and KCTD10(N145) but it barely with KCTD10(C142) or KCTD10(3A) (Fig. 7B). These results suggest that KCTD10 binds to CUL3 principally through the N-terminal BTB domain. In contrast, CEP97 effectively co-precipitated with KCTD10(C142) and KCTD10(3A) but not with KCTD10(N145) (Fig. 7C), suggesting that KCTD10 binds to CEP97 via its C-terminal region.

We then examined whether overexpression of these KCTD10 mutants affects the amount and localization of centrosomal CEP97

Journal of Cell Science (2018) 131, jcs219527. doi:10.1242/jcs.219527

Fig. 6. KCTD10 is required for CEP97 degradation, CP110 removal and ciliogenesis. (A) Knockdown of *KCTD10* blocks ciliogenesis. RPE1 cells were transfected with control or *KCTD10* siRNAs and serum-starved for 48 h. Cells were fixed and stained with anti-CEP97 (green), anti-Ac-tubulin and anti-γ-tubulin (magenta) antibodies. DNA was stained with DAPI (blue). Scale bars: 10 µm. (B) Quantification of the percentage of ciliated cells based on staining for Ac-tubulin. (C) Knockdown of *KCTD10* causes CEP97 accumulation on the centrosome and retention on the mother centriole. RPE1 cells were transfected and serum-starved as in A. Cells were fixed and stained with anti-CEP97 (green), and anti-FOP (magenta) and anti-CEP170 (blue) antibodies. DNA was stained with DAPI (red). Scale bars: 10 µm. (D) Quantification of the percentage of cells with categorized into classes 1–3, as shown in Fig. 3C. (E) Knockdown of *KCTD10* suppresses the removal of CP110 from the mother centriole. RPE1 cells were transfected with siRNAs targeting *KCTD10*. Cells were treated and analyzed, as in Fig. 4A. Scale bars: 10 µm. (F) Quantitative analyses of the percentage of cells with CP110 localized to one centriole. Right panels in A, C and E show magnified images of the white boxes. Outlined and white arrowheads indicate mother and daughter centrioles in C and E, respectively. Data in B, D and F are presented as the mean±s.e.m. from four independent experiments with >100 cells per sample. Statistical significance was calculated using ordinary one-way ANOVAs with Tukey's test. **P*<0.05; ****P*<0.001; *****P*<0.0001. (G) KCTD10 binds to Cep97. HEK293T cells were transfected with CEP97-mCherry and YFP-KCTD10 or YFP. Lysates were precipitated with a GST-tagged anti-GFP nanobody pre-bound to glutathione-Sepharose beads. Beads and lysates were analyzed by immunoblotting with anti-mCherry and anti-GFP antibodies.

and ciliogenesis under serum-starved conditions. Overexpression of YFP-tagged KCTD10(C142) or (3A), but not (N145), significantly decreased the number of class 1 cells with CEP97 localization to a single centriole, and increased the number of class 2 cells with CEP97 localization to two centrioles and class 3 cells with CEP97 accumulation on the centrosome (Fig. 7D,E). Furthermore, overexpression of YFP-KCTD10(C142) or (3A), but not (N145), significantly suppressed ciliogenesis under serum-starved conditions (Fig. 7F). Fluorescence image analyses showed that YFP-KCTD10(C142) and (3A), but not (N145), were enriched on the centrosome (Fig. 7D). These results suggest that KCTD10 mutants (C142 and 3A) have dominant-negative effects on serum-starvation-induced CEP97 degradation and ciliogenesis, and that the interaction between KCTD10 and CUL3 is crucial for CEP97 degradation and ciliogenesis.

By using YFP-KCTD10(WT) and (3A) constructs, we further carried out rescue experiments with *KCTD10* knockdown cells. We generated an siRNA-resistant (sr) silent mutation into YFP-KCTD10 constructs and confirmed the expression of these proteins even in the *KCTD10* siRNA-treated cells (Fig. S7A). Immunostaining for CEP97 showed that expression of sr-KCTD10(WT) partially rescued the reduction of class 1 cells with CEP97 localization to one centriole, whereas expression of sr-KCTD10(3A) had no such effect (Fig. S7B,C). These results further suggest that the KCTD10 BTB domain is required for CEP97 degradation and its removal from the mother centriole.

KCTD10 localizes on the mother centriole

Upon serum starvation, CEP97 and CP110 are removed from the mother centriole but not the daughter centriole. The specific removal of these proteins from the mother centriole might be regulated by the localization of KCTD10 to the mother centriole. To examine this possibility, we analyzed the localization of KCTD10 in RPE1 cells by immunostaining with an anti-KCTD10 antibody. Intriguingly, KCTD10 was localized to one of the two γ-tubulin-positive centrioles in serum-fed cells and at the base of the primary cilium in serum-starved cells (Fig. 8A). KCTD10 was also detected as punctate foci in the nucleus. To examine whether KCTD10 is localized to the mother centriole, we also analyzed KCTD10 localization by co-staining with CEP170, a protein that is localized to the subdistal appendage of the mother centriole and in the transition zone of the primary cilium (Guarguaglini et al., 2005). KCTD10 was located in close proximity to CEP170, indicating that KCTD10 was localized to the mother centriole in serum-fed cells and in the basal region of the cilium in serum-starved cells (Fig. 8B and Fig. S7D). Moreover, the anti-KCTD10 immunostaining signals were diminished by treatment with *KCTD10* siRNAs (Fig. S7D). These results suggest that KCTD10 is specifically localized to the mother centriole where it promotes CEP97 degradation and removal from the mother centriole.

DISCUSSION

CP110 and CEP97 cooperatively function to block unscheduled ciliogenesis in proliferating cells. When cells enter the quiescent phase, these proteins are removed from the mother centriole, which triggers axoneme extension to form primary cilia (Spektor et al., 2007). In this study, we examined the mechanism of quiescence-induced removal of CEP97, and its role in CP110 removal and ciliogenesis. We showed that treatment with MG-132 suppressed serum-starvation-induced degradation of CEP97 and caused aberrant accumulation of CEP97 on the centrosome, indicating that upon serum starvation, centrosomal CEP97 is degraded by the ubiquitin-proteasome system. In fact, CEP97 was preferentially polyubiquitylated in serum-starved cells. Overexpression of a non-ubiquitylatable CEP97(3KR) blocked CP110 removal from the mother centriole and ciliogenesis more severely than did overexpression of CEP97(WT), indicating the crucial role of CEP97 ubiquitylation in those processes. Several steps of screening, by using siRNA-based knockdown experiments and VIP protein-binding assays, revealed that the CUL3–RBX1–KCTD10 complex is the most potent candidate E3 ubiquitin ligase responsible for CEP97 degradation. Depletion of each component of this E3 ligase complex or overexpression of KCTD10 mutants caused dysregulation of CEP97 at the centrosome, suppressed CEP97 removal from the mother centriole and blocked ciliogenesis. Moreover, KCTD10 was selectively localized to the mother centriole. In addition, knockdown of *CUL3*, *RBX1* or *KCTD10* significantly decreased the population of cells with CP110 localized to one centriole under serum-starved conditions. Taken together, these results strongly suggest that the CUL3–RBX1–KCTD10 complex acts as the E3 ligase for CEP97, and plays a crucial role in the removal of CEP97 and CP110 from the mother centriole and in ciliogenesis induced by serum starvation (Fig. 8C).

Knockdown of *CUL3* increased the population of class 2 cells (with CEP97 localization to two centrioles) and class 3 cells (with CEP97 accumulation on the centrosome) and inversely decreased the population of class 1 cells (with CEP97 localization to one centriole, presumably a daughter centriole) (Fig. 3C). The sum of the increase in the percentages of class 2 and class 3 cells (or the decrease in the percentage of class 1 cells) (~50%) was comparable to the drop in the percentage of ciliated cells in *CUL3* knockdown cells (Fig. 3E). Thus, these results suggest that knockdown of *CUL3* causes the defects in ciliogenesis principally by stabilizing centrosomal CEP97 and impairing CEP97 removal from the mother centriole. On the other hand, whereas the percentage of cells with CEP97 localized to one centriole (class 1 cells) was ~40% (Fig. 3C), the percentage of ciliated cells was ~10% (Fig. 3E). Thus, the percentage of cells with CEP97 removed from mother centriole but still no cilium formation is ~30%. This percentage is comparable to that for control siRNA cells, in which the

Journal of Cell Science (2018) 131, jcs219527. doi:10.1242/jcs.219527

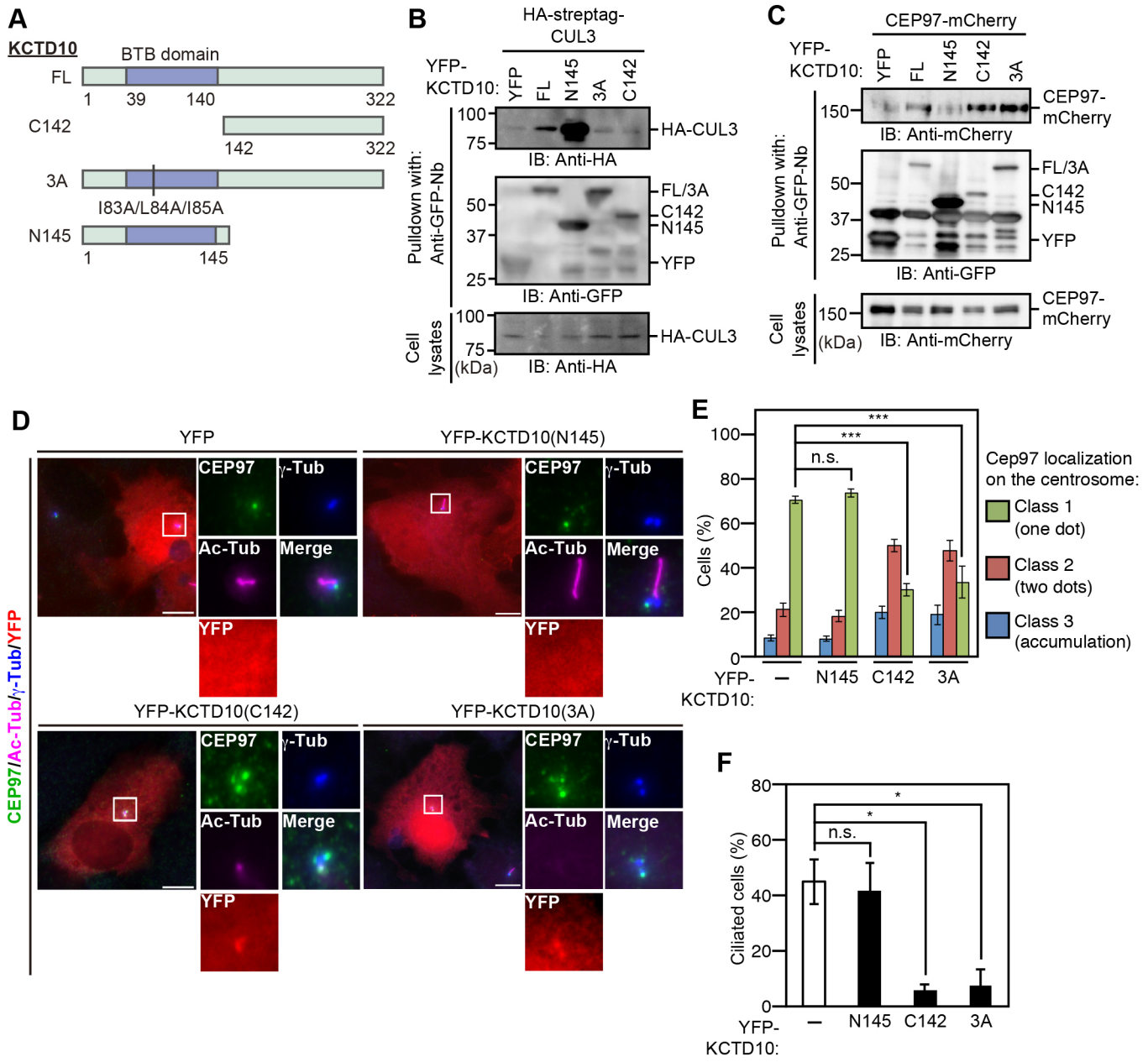

Fig. 7. Expression of KCTD10 mutants causes CEP97 accumulation on the centrosome and retention on the mother centriole, and suppresses ciliogenesis. (A) Schematic structures of KCTD10 and its mutants. Numbers indicate amino acid residues. (B) Co-precipitation assay of CUL3 with KCTD10 mutants. YFP-KCTD10 and its mutants were co-transfected with HA-streptag-CUL3 into HEK293T cells, and the lysates were incubated with a GST-anti-GFP-nanobody (Nb) prebound to glutathione-Sepharose beads. Beads and lysates were analyzed by immunoblotting with anti-HA and anti-GFP antibodies. (C) Co-precipitation assay of CEP97 with KCTD10 mutants. YFP-KCTD10 and its mutants were co-transfected with CEP97-mCherry into HEK293T cells, and the lysates were incubated with a GST-anti-GFP-nanobody prebound to glutathione-Sepharose beads. Beads and lysates were analyzed by immunoblotting with anti-mCherry and anti-GFP antibodies. (D) Overexpression of KCTD10(C142) or KCTD10(3A), but not KCTD10(N145), causes CEP97 accumulation on the centrosome and retention of CEP97 on the mother centrosome, and blocks ciliogenesis in serum-starved cells. RPE1 cells were transfected with YFP or YFP-KCTD10 mutants and serum-starved for 48 h. Cells were fixed and stained with anti-CEP97 (green), anti-Ac-tubulin (magenta) and anti-γ-tubulin (blue) antibodies. Cells were also imaged by YFP fluorescence (red). Right panels show magnified images of the white boxes. Scale bars: 10 µm. (E) Quantification of the percentage of cells categorized into classes 1–3, as shown in Fig. 3C. (F) Quantification of the percentage of ciliated cells. Data in E and F are presented as the mean±s.e.m. from three independent experiments with >50 cells per experiment. Statistical significance was calculated using ordinary one-way ANOVAs with Tukey's test. n.s., not significant; *P<0.05; ***P<0.001.

percentages of class 1 cells and ciliated cells were 80–90% and 60%, respectively. Thus, 20–30% of either control cells or *CUL3*-knockdown cells failed to form cilia even when they lost CEP97 from the mother centriole. These results suggest that CEP97 removal alone is not sufficient for ciliogenesis, and other mechanisms that properly control the following processes, such as axonemal microtubule extension and intraflagellar transport, are required to complete ciliogenesis.

In accordance with previous reports (Spektor et al., 2007), we showed that CEP97 depletion reduced the level of CP110 protein

Journal of Cell Science (2018) 131, jcs219527. doi:10.1242/jcs.219527

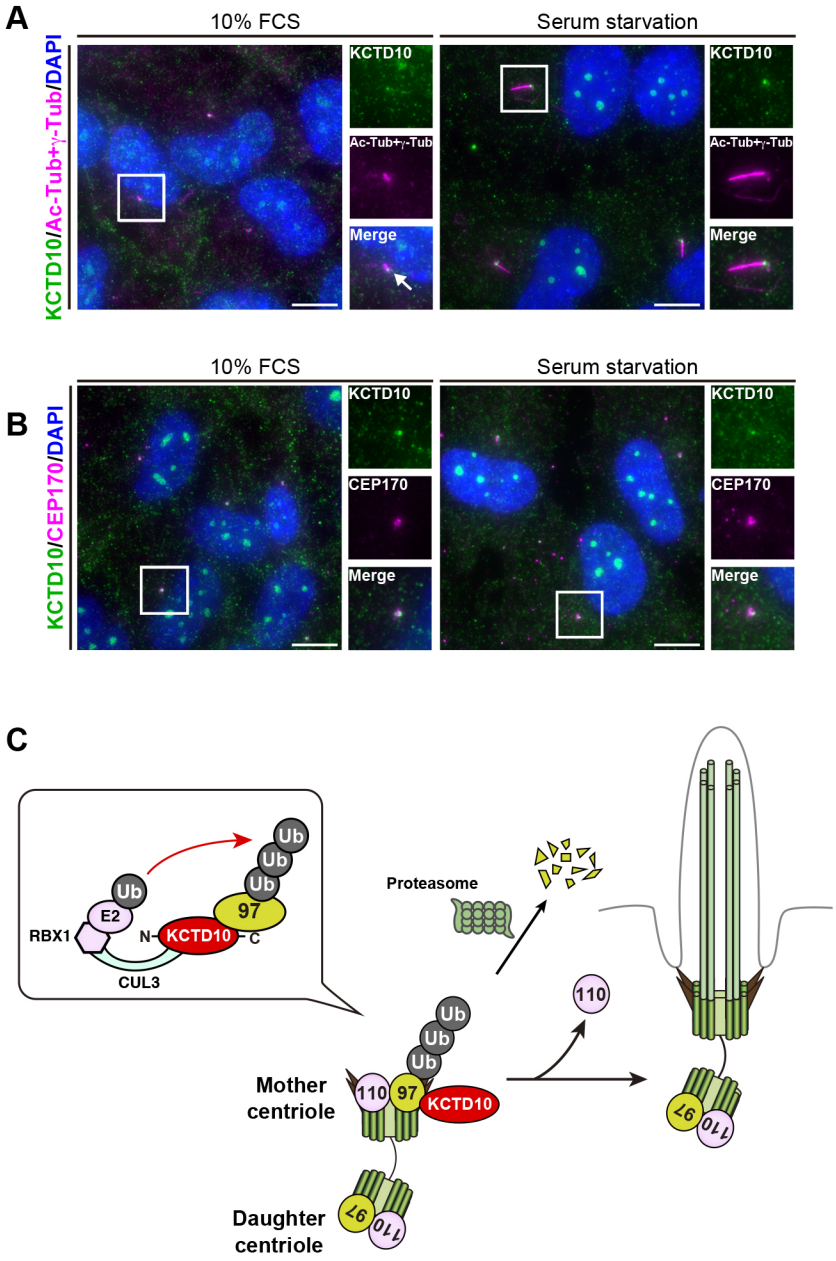

Fig. 8. KCTD10 localizes to the mother centriole. (A) KCTD10 is located on a single centriole and at the base of the primary cilium. RPE1 cells were cultured in the medium containing 10% FCS or under serum-starved conditions for 48 h. Cells were fixed and stained with anti-KCTD10 (green), and anti-Ac-tubulin and anti-γ-tubulin (magenta) antibodies. DNA was stained with DAPI (blue). Right panels show magnified images of the white boxes. Scale bars: 10 µm. An arrow indicates the position of KCTD10 colocalized with γ-tubulin. (B) KCTD10 is located on the CEP170-positive mother centriole. RPE1 cells were cultured under serum-fed and serum-starved conditions as in A. Cells were fixed and stained with anti-KCTD10 (green) and anti-CEP170 (magenta) antibodies. DNA was stained with DAPI (blue). Scale bars: 10 µm. (C) A proposed model of CUL3–RBX1–KCTD10 E3 ligase-mediated CEP97 degradation and its role in ciliogenesis. KCTD10 is localized to the mother centriole and bridges the interaction between CEP97 and the CUL3–RBX1 complex. Upon serum starvation, CEP97 is polyubiquitylated by the CUL3–RBX1–KCTD10 E3 ligase complex and degraded in a proteasome-dependent mechanism. CEP97 degradation leads to CP110 destabilization and removal from the mother centriole and, thereby, induces axoneme extension to form the primary cilium. 97 and 110 are CEP97 and CP110, respectively. Ub, ubiquitin.

and caused CP110 disappearance from the centrioles, indicating that CEP97 plays a crucial role in controlling protein stability and centriolar recruitment of CP110. However, CP110 depletion did not affect CEP97 protein levels but abrogated CEP97 centriolar localization (Spektor et al., 2007), indicating that CP110 is required for CEP97 recruitment to the centrioles but not for its stability. These results suggest that, whereas CEP97 and CP110 are mutually required for their co-recruitment to the centrioles, CEP97 appears to play a dominant role in controlling the stability of the CEP97–CP110 complex on the centrioles. Thus, it is conceivable that CEP97 ubiquitylation and degradation play a key role in the removal of the CEP97–CP110 complex from the mother centriole at the early stage of ciliogenesis.

Previous studies have demonstrated that CP110 is degraded during G2 and M phases, with $SCF^{CyclinF}$ and USP33 mediating ubiquitylation and deubiquitylation of CP110, respectively (D'Angiolella et al., 2010; Li et al., 2013). However, the roles of $SCF^{CyclinF}$ and USP33 in ciliogenesis in quiescent cells have not yet been elucidated. Recent studies demonstrated that EDD-DYRK2-$DDB1^{VprBP}$ and NEURL-4, the E3 ligase components, regulate ubiquitylation and stability of CP110, and that inhibition or depletion of these proteins suppresses ciliogenesis (Hossain et al., 2017; Loukil et al., 2017). In this study, we demonstrated for the first time that CEP97 is degraded in serum-starved cells through the ubiquitin-proteasome system. We also showed that expression of the non-ubiquitylated CEP97(3KR) mutant severely suppressed serum-starvation-induced CP110 removal and ciliogenesis, which strongly suggests that CEP97 ubiquitylation is a prerequisite for CP110 removal and ciliogenesis. Because CEP97 knockdown causes CP110 disappearance, CEP97 degradation is likely to trigger CP110 degradation and removal from the mother centriole. However, further studies are needed to elucidate the precise mechanism of how CEP97 regulates CP110 ubiquitiylation and stability, and the suppressive function of the CEP97–CP110 complex in ciliogenesis.

Knockdown of *CUL3*, *RBX1* or *KCTD10* did not completely suppress the removal of CEP97 and CP110 from the mother centriole but effectively blocked ciliogenesis, suggesting that this E3 complex can have other targets for ciliogenesis. As for CUL3, a previous study has shown that CUL3 promotes ubiquitylation and degradation of trichoplein, a negative regulator of ciliogenesis, through binding to the alternative BTB domain-containing protein KCTD17 (Kasahara et al., 2014). Here, we showed that the CUL3–KCTD10 complex is involved in ciliogenesis by promoting CEP97 degradation. Therefore, CUL3 has, at least, dual roles in ciliogenesis through ubiquitylation of trichoplein and CEP97, mediated by KCTD17 and KCTD10, respectively.

KCTD10 has previously been shown to be a binding partner of B9-domain-containing protein-1 (B9D1), which is localized to the transition zone of the primary cilium, and mutations of which cause ciliopathies (Chih et al., 2012). In fact, we showed here that KCTD10 is specifically localized to the mother centriole in serum-fed cells and to the base of the primary cilium in ciliated cells cultured under serum-starved conditions. The selective localization of KCTD10 to the mother centriole further supports the notion that the CUL3–KCTD10 complex plays a key role in the selective removal of CEP97 from the mother centriole. However, KCTD10 is localized to the mother centriole, irrespective of the presence or absence of serum in culture medium. Thus, the serum-starvation-induced degradation and removal of CEP97 from the mother centriole are not regulated by the translocation of KCTD10. Additional mechanisms are required to activate KCTD10-mediated CEP97 degradation upon serum starvation. Further investigations on the mechanism controlling CUL3–RBX1–KCTD10-mediated CEP97 degradation and removal from the mother centriole during early ciliogenesis will provide a better understanding of quiescence-induced ciliogenesis and pathogenesis of ciliopathies.

MATERIALS AND METHODS

Antibodies and reagents

MG-132 (C2211; MilliporeSigma, St Louis, MO), 4′,6-diamidino-2-phenylindole (DAPI) (09224; Polysciences, Warrington, PA), MLN4924 (I-502; Boston Biochem, Cambridge, MA), Heclin (5433/10; R&D Systems, Minneapolis, MN), VH298 (6156/10; R&D Systems) and horseradish peroxidase-conjugated streptavidin (SA-5004; Vector Laboratories, Burlingame, CA) were purchased from indicated suppliers. Antibodies were purchased as follows: rabbit polyclonal antibodies against CEP97 (Novus Biologicals, Littleton, CO), CP110 (Bethyl Laboratories, Montgomery, TX), GFP (Thermo Fisher Scientific, Waltham, MA), KCTD10 (Novus Biologicals), Arl13b, CUL1, CUL2, CUL4A, CUL4B and CUL7 (Proteintech, Rosemont, IL), CUL3 (Cell Signaling, Danvers, MA), Centrin (MilliporeSigma), RBX1 and mCherry (Genetex, Irvine, CA); mouse monoclonal antibodies against CEP170 (Thermo Fisher Scientific), β-actin, α-tubulin, γ-tubulin and acetylated (Ac)-tubulin (MilliporeSigma), Myc-tag (Medical & Biological Laboratories, Nagoya, Japan), CUL5 (Santa Cruz Biotechnology, Dallas, TX) and FOP (Abnova, Taipei, Taiwan); Alexa488-conjugated mouse monoclonal antibody against Ki-67 (BioLegend, San Diego, CA); rat monoclonal antibody against HA (MilliporeSigma); HRP-conjugated sheep anti-mouse IgG, donkey anti-rabbit IgG or goat anti-rat IgG (GE Healthcare, Chalfont St Giles, UK), Alexa350, Alexa488, Alexa568, Alexa633 or Alexa647-conjugated goat anti-mouse IgG, goat anti-mouse IgG1, goat anti-mouse IgG2b or goat anti-rabbit IgG (Thermo Fisher Scientific). Detailed information about antibodies used in this study is shown in Table S3.

Plasmids

Human cDNAs for CEP97 and CP110 were provided by Tetsuo Kobayashi (Nara Institute of Science and Technology, Ikoma, Japan) and Brian D. Dynlacht (New York University, New York, NY). Plasmids encoding HA-ubiquitin (#18712), HA-streptag-CUL3 (#36970) and HA-RBX1 (#19897) were purchased from Addgene. The human cDNA for CUL1 was cloned by PCR amplification. To screen for CEP97 E3 ligase, we selected 179 genes encoding BTB domain-containing proteins by searching Swiss-Prot database and a previous report (Stogios et al., 2005). Of these 179 genes, we used 150 genes in this study; and of those, 29 genes had two variant clones in a HuPEX library (Maruyama et al., 2012) (Table S1). DNA of 101 clones was each inserted into the pDESTMN-Venus206K mammalian expression vector. DNA of 78 clones was each inserted into pENTR vector, and the resulting 78 cDNAs were transferred into the pDESTMN-Venus206K vector in an LR reaction using a GATEWAY LR clonase mix (#11791-043; Thermo Fisher Scientific). The cDNA plasmids for mutants of CEP97 and KCTD10 were constructed using a site-directed mutagenesis kit (Agilent, Santa Clara, CA). The cDNA plasmid for siRNA-resistant (sr)-KCTD10 was constructed by introducing three silent mutations into a target sequence of KCTD10 siRNA (5′-GAAGCA-CTTTGGCACCATC-3′, mutated nucleotides are underlined) by using a site-directed mutagenesis kit (Agilent).

siRNAs

The list of siRNAs used in this study is shown in Table S4. Silencer negative control siRNA (4390843; Thermo Fisher Scientific) and ON-TARGETplus non-targeting siRNA (D-001810-01-05; GE Dharmacon, Lafayette, CO) were used as control siRNA #1 and #2, respectively. In knockdown experiments, we quantified the effects of knockdown based on the premise that siRNAs were effectively transfected into almost all cells, since we observed that CUL3 siRNAs grossly reduced the fluorescence intensity of anti-CUL3 immunostaining in almost all cells on the plate (Fig. S8).

Cell culture and transfection

Human telomerase reverse transcriptase-immortalized retinal pigmented epithelial (RPE)-1 cells were provided by Hiroyuki Nakanishi (Kumamoto University, Kumamoto, Japan). Cells had recently been authenticated and tested for contamination. RPE1 cells were cultured in Dulbecco's modified Eagle's medium (DMEM)/Ham's F-12 (042-30555; Wako Pure Chemical, Osaka, Japan) supplemented with 10% fetal calf serum (FCS; Biosera, Kansas City, MO). HEK293T cells obtained from ATCC (No. CRL-3216; Manassas, VA) were cultured in DMEM (044-29765; Wako Pure Chemical) supplemented with 10% FCS. Both cell lines were tested for mycoplasma contamination and found to be negative. Transfection with plasmids was performed using Lipofectamine LTX with PLUS reagent (Thermo Fisher Scientific) in RPE1 cells, and FuGENE HD (Promega, Madison, WI) or JetPEI (PolyPlus, New York, NY) in HEK293T cells. Transfection with siRNAs was performed using Lipofectamine RNAiMAX (Thermo Fisher Scientific). For knockdown experiments, RPE1 cells were plated on coverslips in 6-well culture plates at an average density of 1.0×10^4 cells/cm^2. At 24 h after transfection, cells were serum-starved for 48 h before fixation. For rescue experiments, RPE1 cells were plated on coverslips in 6-well culture plates at an average density of 1.0×10^4 cells/cm^2, transfected with plasmids and cultured for 4 h. Then, cells were transfected with siRNAs, cultured for 24 h and serum-starved for 48 h before fixation. To examine the effects of MG-132 or E3 ligase inhibitors, RPE1 cells were plated on coverslips in 6-well culture plates at high density of 3.5×10^4 cells/ cm^2 and serum starved for 24 h. Exposure of 0.3 µM MG-132, 0.5 µM MLN4924, 100 µM Heclin or 100 µM VH298 was carried out for 24 h before fixation or cell harvesting.

Immunoblotting

Immunoblotting was carried out as described previously (Nagai et al., 2013; Nagai and Mizuno, 2017). To examine the levels of CEP97 protein, cells were lysed with lysis buffer (150 mM NaCl, 50 mM HEPES-KOH pH 7.2, 1 mM $MgCl_2$, 1% Triton X-100, 1 mM PMSF, 10 µg/ml leupeptin, 3 µg/ml pepstatin, 10 µM E-64). To examine CEP97 phosphorylation, MG-132-treated cell lysates were incubated with 0.25 U/µl of λ-phosphatase (New England BioLabs, Ipswich, MA). Proteins were transferred to Immobilon-P (MilliporeSigma) polyvinylidene difluoride membrane using semi-dry transfer apparatus (BE-300. BIO CRAFT, Tokyo, Japan) according to the

manufacturer's instructions. Protein-transferred membranes were subjected to immunoblot analyses using a standard protocol.

Quantitative RT-PCR

Total RNA was isolated from RPE1 cells using an Isogen II kit (Nippon Gene, Tokyo, Japan). One µg total RNA was subject to reverse transcription to yield single-stranded cDNAs using a PrimeScript RT Reagent Kit (TaKaRa, Shiga, Japan). For quantitative PCR, cDNA fragments were amplified using SYBR Premix Ex Taq II (TaKaRa) and the products was detected by Applied Biosystems 7300 (Thermo Fisher Scientific). All reactions were done according to the manufacturer's instruction. Sequences of primers for quantitative PCR are shown in Table S5. Analyses of the data were done using 7300 System Software (Thermo Fisher Scientific) and Microsoft Excel (Microsoft, Redmond, WA).

Immunostaining and fluorescence microscopy

Immunostaining was carried out as described previously (Oda et al., 2014). Cells were fixed with 4% paraformaldehyde in phosphate-buffered saline (PBS) followed by methanol fixation or with methanol alone. Cells were stained with primary antibody diluted with Can-Get-Signal Immunostain (Toyobo, Osaka, Japan) and secondary antibody diluted with 2% FCS in PBS. Fluorescence images were obtained using a DMI6000B fluorescence microscope (Leica Microsystems, Wetzlar, Germany) equipped with a PL Apo 63× and 100× oil objective lens and CCD camera (Cool SNAP HQ, Roper Scientific, Vianen, The Netherlands). Image acquisition was performed using LAS AF software (Leica Microsystems). Image processing was performed using ImageJ (NIH, Bethesda, MD).

Immunoprecipitation

Immunoprecipitation was performed as described previously (Toshima et al., 2001). Briefly, cells were lysed with lysis buffer (150 mM NaCl, 50 mM HEPES-KOH pH 7.2, 1 mM $MgCl_2$, 1% Triton X-100, 1 mM PMSF, 10 µg/ml leupeptin, 3 µg/ml pepstatin, 10 µM E-64) and centrifuged. Lysates were pre-cleared with Protein A-Sepharose (GE Healthcare) for 1 h at 4°C, and the supernatants were incubated with antibodies and Protein A-Sepharose or GST-anti-GFP-nanobody pre-bound to glutathione-Sepharose beads (GE Healthcare) for 4 h at 4°C. After centrifugation, immunoprecipitates were washed three times and used for the immunoblot analysis. Detection of protein polyubiquitylation was performed as described previously (Yatsu et al., 2015). Briefly, cells were treated with 10 µM MG-132 before harvesting and lysed with lysis buffer (150 mM NaCl, 50 mM HEPES-KOH pH 7.2, 1 mM $MgCl_2$, 1% Triton X-100, 1 mM PMSF, 10 µg/ml leupeptin, 3 µg/ml pepstatin, 10 µM E-64, 10 mM *N*-ethylmaleimide) and centrifuged. Lysates were pre-cleared with Protein A-Sepharose for 1 h at 4°C and the supernatants were incubated with antibodies and Protein A-Sepharose or GST-anti-mCherry-nanobody prebound to glutathione-Sepharose beads (GE Healthcare) for 2 h at 4°C. After centrifugation, immunoprecipitates were washed twice and used for the immunoblot analysis.

VIP assay

VIP assay was performed as described previously (Katoh et al., 2015). Briefly, HEK293T cells were co-transfected with plasmids encoding CEP97-mCherry and Venus-tagged BTB domain-containing proteins and cultured for 2 days. Cells were lysed with HNTG buffer (150 mM NaCl, 20 mM HEPES-KOH pH 7.4, 0.1% Triton X-100, 10% glycerol, 1 mM PMSF, 10 µg/ml leupeptin, 3 µg/ml pepstatin, 10 µM E-64) and incubated on ice for 15 min. After centrifugation, supernatants were incubated with GST-anti-mCherry nanobody–prebound glutathione-Sepharose 4B (GE Healthcare) for 1 h at 4°C. Precipitates were washed with HNTG buffer three times and then transferred into a 96-well plate. Fluorescence on the beads was observed using a DMI6000B fluorescence microscope (Leica Microsystems) equipped with a C PLAN L20× dry objective lens and CCD camera (Cool SNAP HQ, Roper Scientific). Image acquisition was performed using LAS AF software (Leica Microsystems). Image processing was performed using ImageJ (NIH). A protein was considered as a candidate if its Venus fluorescence on the beads was more intense than that of YFP-CP110 beads.

Statistical analyses

All statistical analyses were carried out by Prism 6 (GraphPad Software, La Jolla, CA). Data are expressed as the mean±standard error of the mean (±s.e.m.) of at least three independent experiments. Sample size and number of repeated experiments are described in figure legends. *P*-values were calculated using the Student's *t*-test for two-group comparisons and one-way ANOVA followed by the Tukey's test for multiple data set comparisons. All statistical analyses were conducted with a significance level of α=0.05 (P<0.05).

Acknowledgements

We thank Kazuki Irie, Shinya Umeda, Yo Hasegawa and Ryo Tamura (Tohoku University, Sendai, Japan) for technical assistance. We also thank Dr Tadashi Nakagawa and Dr Keiko Nakayama (Tohoku University) for helpful advice, Dr Yohei Kato and Dr Kazuhisa Nakayama (Kyoto University, Kyoto, Japan) for helpful advice and for providing the cDNA plasmids for GST-tagged anti-GFP and anti-mCherry-nanobodies, Dr Tetsuo Kobayashi (Nara Institute of Science and Technology, Ikoma, Japan) and Dr Brian D. Dynlacht (New York University, New York, NY) for providing cDNAs for CEP97 and CP110, and Dr Hiroyuki Nakanishi (Kumamoto University, Kumamoto, Japan) for providing RPE1 cells.

Competing interests

The authors declare no competing or financial interests.

Author contributions

Conceptualization: T.N., S.M., K.M.; Methodology: T.N., S.M.; Validation: T.N., S.M., K.M.; Investigation: T.N., S.M.; Resources: T.N., S.M., H.K., N.G., K.M.; Data curation: T.N., S.M.; Writing - original draft: T.N., K.M.; Writing - review & editing: T.N., K.M.; Visualization: T.N., S.M.; Supervision: K.M.; Project administration: K.M.; Funding acquisition: T.N., K.M.

Funding

This work was supported by Grants-in-aid for Scientific Research from the Japan Society for the Promotion of Science, KAKENHI [15H04347, 15H01197 and 18H02398 to K.M., and 16K20910 to T.N.].

Data availability

All data supporting the findings of this study are available from the corresponding author on request.

Supplementary information

Supplementary information available online at
http://jcs.biologists.org/lookup/doi/10.1242/jcs.219527.supplemental

References

Basten, S. G. and Giles, R. H. (2013). Functional aspects of primary cilia in signaling, cell cycle and tumorigenesis. *Cilia* **2**, 6.

Bettencourt-Dias, M. and Carvalho-Santos, Z. (2008). Double life of centrioles: CP110 in the spotlight. *Trends Cell Biol.* **18**, 8-11.

Cao, J., Shen, Y., Zhu, L., Xu, Y., Zhou, Y., Wu, Z., Li, Y., Yan, X. and Zhu, X. (2012). miR-129-3p controls cilia assembly by regulating CP110 and actin dynamics. *Nat. Cell Biol.* **14**, 697-706.

Chen, Y., Yang, Z., Meng, M., Zhao, Y., Dong, N., Yan, H., Liu, L., Ding, M., Peng, H. B. and Shao, F. (2009). Cullin mediates degradation of RhoA through evolutionarily conserved BTB adaptors to control actin cytoskeleton structure and cell movement. *Mol. Cell* **35**, 841-855.

Chih, B., Liu, P., Chinn, Y., Chalouni, C., Komuves, L. G., Hass, P. E., Sandoval, W. and Peterson, A. S. (2012). A ciliopathy complex at the transition zone protects the cilia as a privileged membrane domain. *Nat. Cell Biol.* **14**, 61-72.

Cullinan, S. B., Gordan, J. D., Jin, J., Harper, J. W. and Diehl, J. A. (2004). The Keap1-BTB protein is an adaptor that bridges Nrf2 to a Cul3-based E3 ligase: oxidative stress sensing by a Cul3-Keap1 ligase. *Mol. Cell Biol.* **24**, 8477-8486.

D'Angiolella, V., Donato, V., Vijayakumar, S., Saraf, A., Florens, L., Washburn, M. P., Dynlacht, B. and Pagano, M. (2010). SCF(Cyclin F) controls centrosome homeostasis and mitotic fidelity through CP110 degradation. *Nature* **466**, 138-142.

Fliegauf, M., Benzing, T. and Omran, H. (2007). When cilia go bad: cilia defects and ciliopathies. *Nat. Rev. Mol. Cell Biol.* **8**, 880-893.

Frost, J., Galdeano, C., Soares, P., Gadd, M. S., Grzes, K. M., Ellis, L., Epemolu, O., Shimamura, S., Bantscheff, M., Grandi, P. et al. (2016). Potent and selective chemical probe of hypoxic signalling downstream of HIF-alpha hydroxylation via VHL inhibition. *Nat. Commun.* **7**, 13312.

Furukawa, M., He, Y. J., Borchers, C. and Xiong, Y. (2003). Targeting of protein ubiquitination by BTB-Cullin 3-Roc1 ubiquitin ligases. *Nat. Cell Biol.* **5**, 1001-1007.

Genschik, P., Sumara, I. and Lechner, E. (2013). The emerging family of CULLIN3-RING ubiquitin ligases (CRL3s): cellular functions and disease implications. *EMBO J.* **32**, 2307-2320.
Gerdes, J. M., Davis, E. E. and Katsanis, N. (2009). The vertebrate primary cilium in development, homeostasis, and disease. *Cell* **137**, 32-45.
Goetz, S. C. and Anderson, K. V. (2010). The primary cilium: a signalling centre during vertebrate development. *Nat. Rev. Genet.* **11**, 331-344.
Goetz, S. C., Liem, K. F. and Anderson, K. V. (2012). The spinocerebellar ataxia-associated gene Tau tubulin kinase 2 controls the initiation of ciliogenesis. *Cell* **151**, 847-858.
Guarguaglini, G., Duncan, P. I., Stierhof, Y. D., Holmström, T., Duensing, S. and Nigg, E. A. (2005). The forkhead-associated domain protein Cep170 interacts with Polo-like kinase 1 and serves as a marker for mature centrioles. *Mol. Biol. Cell* **16**, 1095-1107.
Hershko, A. and Ciechanover, A. (1998). The ubiquitin system. *Annu. Rev. Biochem.* **67**, 425-479.
Hossain, D., Javadi Esfehani, Y., Das, A. and Tsang, W. Y. (2017). Cep78 controls centrosome homeostasis by inhibiting EDD-DYRK2-DDB1^{VprBP}. *EMBO Rep.* **18**, 632-644.
Izawa, I., Goto, H., Kasahara, K. and Inagaki, M. (2015). Current topics of functional links between primary cilia and cell cycle. *Cilia* **4**, 12.
Kasahara, K., Kawakami, Y., Kiyono, T., Yonemura, S., Kawamura, Y., Era, S., Matsuzaki, F., Goshima, N. and Inagaki, M. (2014). Ubiquitin-proteasome system controls ciliogenesis at the initial step of axoneme extension. *Nat. Commun.* **5**, 5081.
Katoh, Y., Nozaki, S., Hartanto, D., Miyano, R. and Nakayama, K. (2015). Architectures of multisubunit complexes revealed by a visible immunoprecipitation assay using fluorescent fusion proteins. *J. Cell Sci.* **128**, 2351-2362.
Kobayashi, T. and Dynlacht, B. D. (2011). Regulating the transition from centriole to basal body. *J. Cell Biol.* **193**, 435-444.
Kuhns, S., Schmidt, K. N., Reymann, J., Gilbert, D. F., Neuner, A., Hub, B., Carvalho, R., Wiedemann, P., Zentgraf, H., Erfle, H. et al. (2013). The microtubule affinity regulating kinase MARK4 promotes axoneme extension during early ciliogenesis. *J. Cell Biol.* **200**, 505-522.
Lee, J. Y. and Stearns, T. (2013). FOP is a centriolar satellite protein involved in ciliogenesis. *PLoS ONE* **8**, e58589.
Li, J., D'Angiolella, V., Seeley, E. S., Kim, S., Kobayashi, T., Fu, W., Campos, E. I., Pagano, M. and Dynlacht, B. D. (2013). USP33 regulates centrosome biogenesis via deubiquitination of the centriolar protein CP110. *Nature* **495**, 255-259.
Loukil, A., Tormanen, K. and Sütterlin, C. (2017). The daughter centriole controls ciliogenesis by regulating Neurl-4 localization at the centrosome. *J. Cell Biol.* **216**, 1287-1300.
Maruyama, Y., Kawamura, Y., Nishikawa, T., Isogai, T., Nomura, N. and Goshima, N. (2012). HGPD: human gene and protein database, 2012 update. *Nucleic Acids Res.* **40**, D924-D929.
Mertins, P., Qiao, J. W., Patel, J., Udeshi, N. D., Clauser, K. R., Mani, D. R., Burgess, M. W., Gillette, M. A., Jaffe, J. D. and Carr, S. A. (2013). Integrated proteomic analysis of post-translational modifications by serial enrichment. *Nat. Methods* **10**, 634-637.
Mund, T., Lewis, M. J., Maslen, S. and Pelham, H. R. (2014). Peptide and small molecule inhibitors of HECT-type ubiquitin ligases. *Proc. Natl. Acad. Sci. USA* **111**, 16736-16741.
Nagai, T. and Mizuno, K. (2017). Jasplakinolide induces primary cilium formation through cell rounding and YAP inactivation. *PLoS ONE* **12**, e0183030.
Nagai, T., Ikeda, M., Chiba, S., Kanno, S.-I. and Mizuno, K. (2013). Furry promotes acetylation of microtubules in the mitotic spindle by inhibition of SIRT2 tubulin deacetylase. *J. Cell Sci.* **126**, 4369-4380.
Nigg, E. A. and Raff, J. W. (2009). Centrioles, centrosomes, and cilia in health and disease. *Cell* **139**, 663-678.
Oda, T., Chiba, S., Nagai, T. and Mizuno, K. (2014). Binding to Cep164, but not EB1, is essential for centriolar localization of TTBK2 and its function in ciliogenesis. *Genes Cells* **19**, 927-940.
Pan, Z.-Q., Kentsis, A., Dias, D. C., Yamoah, K. and Wu, K. (2004). Nedd8 on cullin: building an expressway to protein destruction. *Oncogene* **23**, 1985-1997.
Petroski, M. D. and Deshaies, R. J. (2005). Function and regulation of cullin-RING ubiquitin ligases. *Nat. Rev. Mol. Cell Biol.* **6**, 9-20.
Pinkas, D. M., Sanvitale, C. E., Bufton, J. C., Sorrell, F. J., Solcan, N., Chalk, R., Doutch, J. and Bullock, A. N. (2017). Structural complexity in the KCTD family of Cullin3-dependent E3 ubiquitin ligases. *Biochem. J.* **474**, 3747-3761.
Prosser, S. L. and Morrison, C. G. (2015). Centrin2 regulates CP110 removal in primary cilium formation. *J. Cell Biol.* **208**, 693-701.
Sánchez, I. and Dynlacht, B. D. (2016). Cilium assembly and disassembly. *Nat. Cell Biol.* **18**, 711-717.
Song, R., Walentek, P., Sponer, N., Klimke, A., Lee, J. S., Dixon, G., Harland, R., Wan, Y., Lishko, P., Lize, M. et al. (2014). miR-34/449 miRNAs are required for motile ciliogenesis by repressing cp110. *Nature* **510**, 115-120.
Soucy, T. A., Smith, P. G., Milhollen, M. A., Berger, A. J., Gavin, J. M., Adhikari, S., Brownell, J. E., Burke, K. E., Cardin, D. P., Critchley, S. et al. (2009). An inhibitor of NEDD8-activating enzyme as a new approach to treat cancer. *Nature* **458**, 732-736.
Spektor, A., Tsang, W. Y., Khoo, D. and Dynlacht, B. D. (2007). Cep97 and CP110 suppress a cilia assembly program. *Cell* **130**, 678-690.
Stogios, P. J., Downs, G. S., Jauhal, J. J. S., Nandra, S. K. and Privé, G. G. (2005). Sequence and structural analysis of BTB domain proteins. *Genome Biol.* **6**, R82.
Thoma, C. R., Frew, I. J., Hoerner, C. R., Montani, M., Moch, H. and Krek, W. (2007). pVHL and GSK3beta are components of a primary cilium-maintenance signalling network. *Nat. Cell Biol.* **9**, 588-595.
Toshima, J. Y., Toshima, J., Watanabe, T. and Mizuno, K. (2001). Binding of 14-3-3β regulates the kinase activity and subcellular localization of testicular protein kinase 1. *J. Biol. Chem.* **276**, 43471-43481.
Tsang, W. Y. and Dynlacht, B. D. (2013). CP110 and its network of partners coordinately regulate cilia assembly. *Cilia* **2**, 9.
Villumsen, B. H., Danielsen, J. R., Povlsen, L., Sylvestersen, K. B., Merdes, A., Beli, P., Yang, Y.-G., Choudhary, C., Nielsen, M. L., Mailand, N. et al. (2013). A new cellular stress response that triggers centriolar satellite reorganization and ciliogenesis. *EMBO J.* **32**, 3029-3040.
Wang, L., Lee, K., Malonis, R., Sanchez, I. and Dynlacht, B. D. (2016). Tethering of an E3 ligase by PCM1 regulates the abundance of centrosomal KIAA0586/Talpid3 and promotes ciliogenesis. *eLife* **5**, e12950.
Wu, K., Fuchs, S. Y., Chen, A., Tan, P., Gomez, C., Ronai, Z. and Pan, Z.-Q. (2000). The SCF(HOS/beta-TRCP)-ROC1 E3 ubiquitin ligase utilizes two distinct domains within CUL1 for substrate targeting and ubiquitin ligation. *Mol. Cell Biol.* **20**, 1382-1393.
Xu, L., Wei, Y., Reboul, J., Vaglio, P., Shin, T.-H., Vidal, M., Elledge, S. J. and Harper, J. W. (2003). BTB proteins are substrate-specific adaptors in an SCF-like modular ubiquitin ligase containing CUL-3. *Nature* **425**, 316-321.
Yatsu, A., Shimada, H., Ohbayashi, N. and Fukuda, M. (2015). Rab40C is a novel Varp-binding protein that promotes proteasomal degradation of Varp in melanocytes. *Biol. Open* **4**, 267-275.

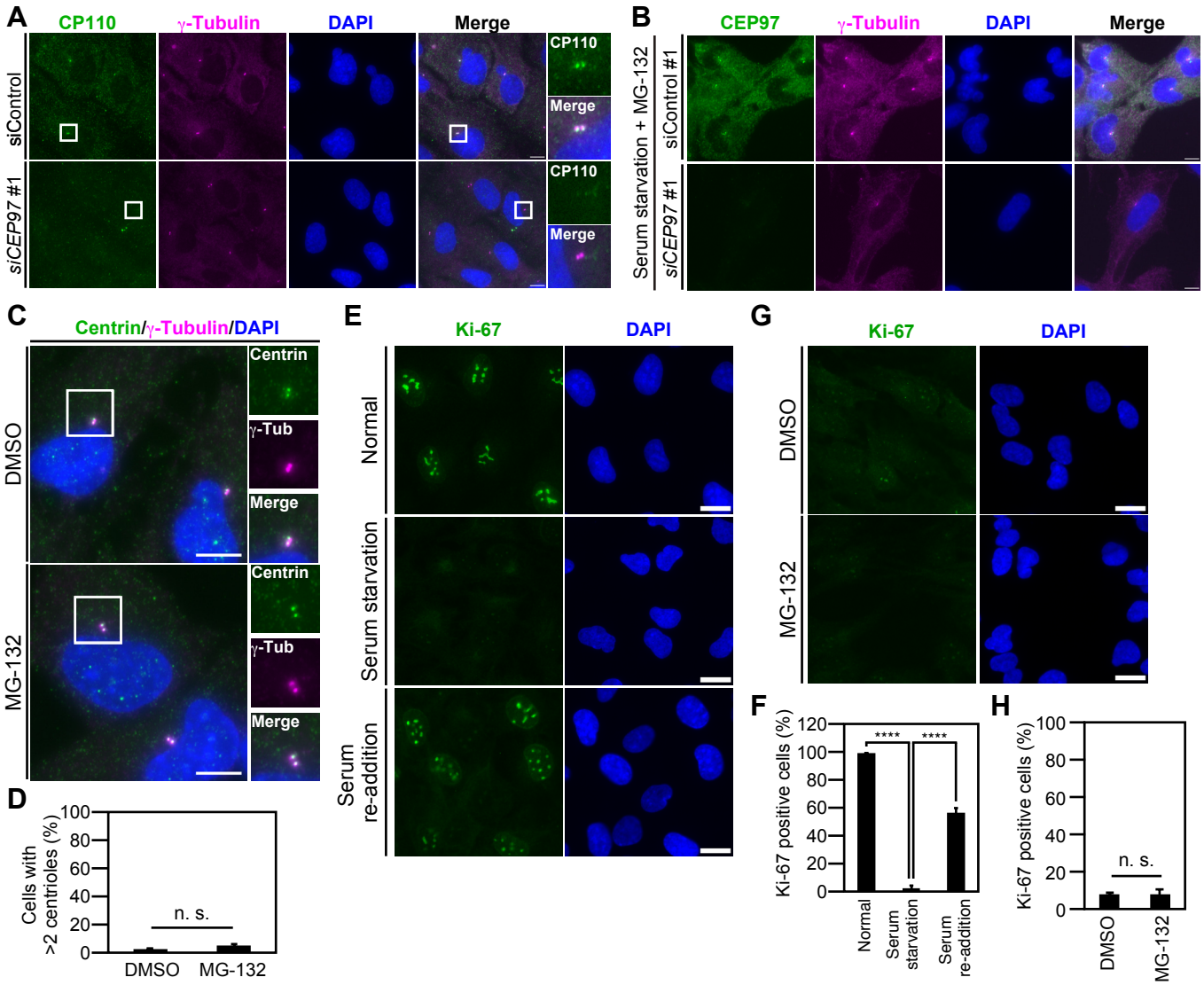

Fig. S1. The disappearance of CP110 from the centrioles by *CEP97* knockdown and the effects of MG-132 treatment on the number of centrioles and cell quiescence. (A) Effect of *CEP97* knockdown on CP110 localization. RPE1 cells were transfected with control or *CEP97* siRNA and cultured in 10% fetal calf serum (FCS)-containing medium for 48 h. Cells were then fixed and stained with anti-CP110 (green) and anti-γ-tubulin (magenta) antibodies. DNA was stained with DAPI (blue). (B) Assessment of the specificity of anti-CEP97 immunostaining by the treatment with *CEP97* siRNA. RPE1 cells were transfected with control or *CEP97* siRNA and treated with 0.3 μM MG-132 in 0.2% FCS-containing medium for 24 h. Cells were fixed and stained with anti-CEP97 (green) and anti-γ-tubulin (magenta) antibodies and DAPI (blue). Scale bar, 10 μm. (C) Effect of MG-132 treatment on the number of centrioles in serum-starved cells. RPE1 cells were serum-starved for 24 h and then treated with 0.3 μM MG-132 or control DMSO in 0.2% FCS-containing medium for 24 h. Cells were fixed and stained with anti-centrin (green) and anti-γ-tubulin (magenta) antibodies and DAPI (blue). In (A) and (C), right panels show magnified images of the white boxes. Scale bar, 10 μm. (D) Quantification of the percentage of cells with >2 centrin/γ-tubulin double-positive foci in MG-132- or DMSO-treated RPE1 cells. Data are means ± SEM from three independent experiments with >100 cells per each sample. (E) Effect of serum starvation on Ki-67 staining. RPE1 cells were cultured in medium containing 10% FCS (Normal), or in medium containing 0.2% FCS (Serum starvation) for 48 h, or cultured in medium containing 0.2% FCS for 24 h and then cultured in medium containing 10% FCS (Serum re-addition). Cells were fixed and stained with Alexa 488-conjugated anti-Ki-67 antibodies (green) and DAPI (blue). Scale bar, 20 μm. (F) Quantification of Ki-67-positive cells in (E). Data are means ± SEM from three independent experiments with >200 cells per each sample. (G) Effect of MG-132 treatment on cell quiescence in serum-starved cells. RPE1 cells were treated as in (C). Cells were fixed as in (E). Scale bar, 20 μm. (H) Quantification of Ki-67-positive cells in (G). Data are means ± SEM from three independent experiments with >200 cells per each sample. In (D), (F) and (H), statistical significance was calculated using two-tailed Student's t-test or ordinary one-way ANOVAs with Tukey's test. n.s., not significant; ****, $P < 0.0001$.

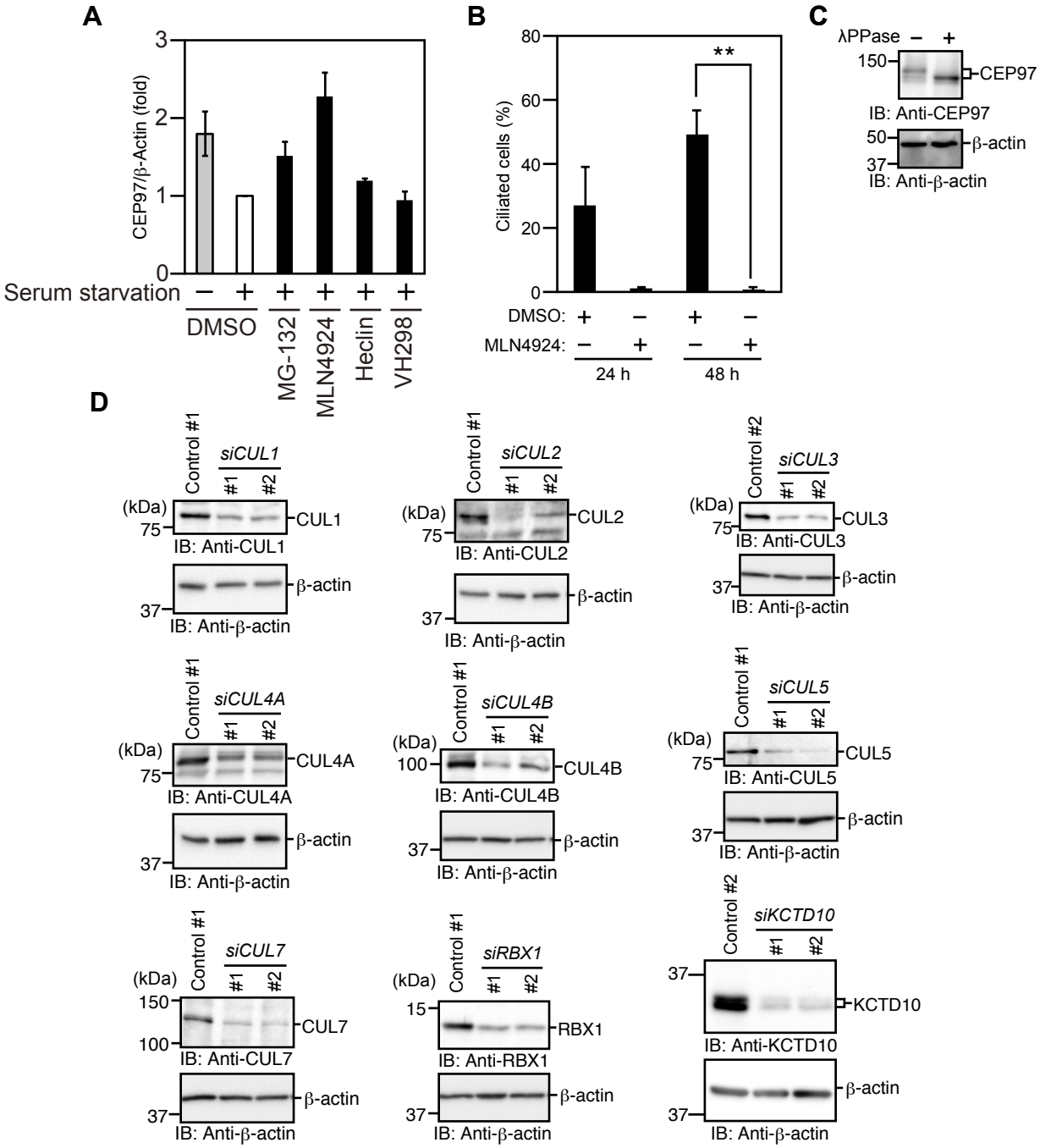

Fig. S2. Effects of E3 ligase inhibitors on the level of CEP97 protein, MLN4924 on ciliogenesis, and λ-phosphatase treatment on CEP97 gel mobility shift, and the knockdown efficiency of siRNAs. (A) Effects of E3 ligase inhibitors on the level of CEP97 protein. The relative ratios of CEP97 to β-actin were measured by densitometric analyses of the CEP97 and β-actin immunoblot data shown in Fig 3A. Data are means ± SEM from four independent experiments. (B) Effect of MLN4924 on ciliogenesis. RPE1 cells were treated with 0.5 μM MLN4924 in 0.2% serum-containing medium for indicated times, and the percentage of ciliated cells was counted. Data are means ± SEM from three independent experiments with >100 cells per each sample. Statistical significance was calculated using two-tailed Student's t-test. **, $P < 0.01$. (C) Effect of λ-phosphatase treatment on the gel mobility shift of CEP97. RPE1 cells were treated with 0.3 μM MG-132 in 0.2% serum-containing medium for 24 h. Cell lysates were incubated in the presence or absence of λ-phosphatase (λPPase) at 30ºC for 2 h, and then analyzed by immunoblotting with anti-CEP97 and anti-β-actin antibodies. (D) Immunoblot analyses of the knockdown efficiency of siRNAs. RPE1 cells were transfected with control siRNA or two indendent siRNAs targeting each *Cullin*, *RBX1* or *KCTD10*, and cultured for 48 h. Cell lysates were analyzed by immunoblotting with indicated antibodies.

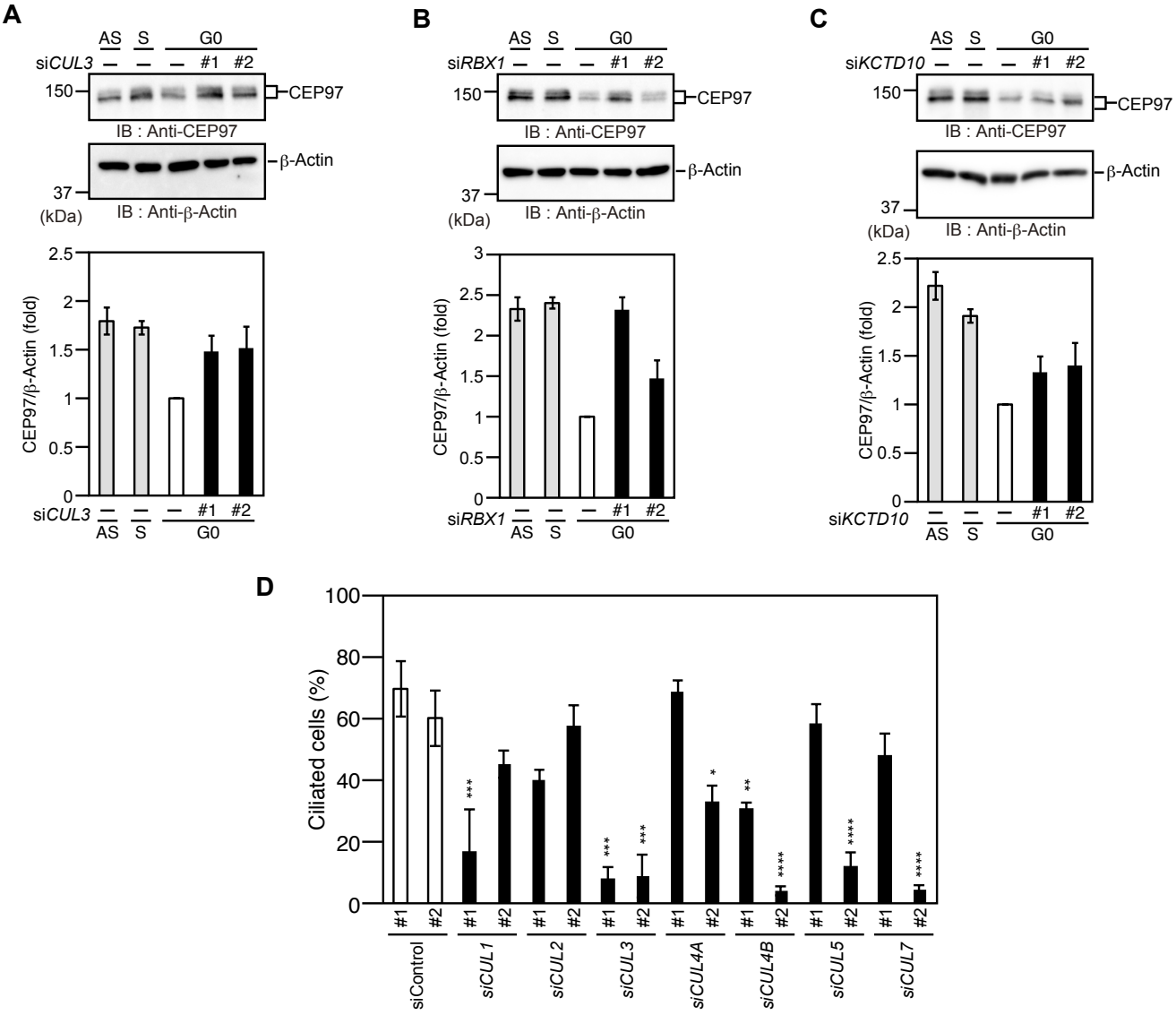

Fig. S3. Effects of *CUL3*, *RBX1* or *KCTD10* knockdown on the level of CEP97 protein and effects of knockdown of each *Cullin* member on ciliogenesis. (A-C) Effects of knockdown on the level of CEP97 protein. RPE1 cells were transfected with control siRNA or two indendent siRNAs targeting *CUL3* (A), *RBX1* (B), or *KCTD10* (C), and cultured in the medium containing 10% fetal calf serum (FCS) (AS, asynchronized), 10% FCS and 2 mM thymidine (S phase arrest), or 0.2% FCS (G0 phase) for 36 h. Cell lysates were analyzed by immunoblotting with anti-CEP97 and anti-β-actin antibodies. Lower panels show the relative ratios of CEP97 to β-actin, as measured by densitometric analyses of CEP97 and β-actin immunoreactive bands. Data are means ± SEM from seven independent experiments. (D) Effects of knockdown of each *Cullin* member on ciliogenesis. RPE1 cells were transfected with control siRNA or two indendent siRNAs targeting each *Cullin*, and cultured for 48 h in serum-starved conditions. Cells were fixed and stained with anti-Ac-tubulin and anti-γ-tubulin antibodies, and the percentages of ciliated cells were counted. Data are means ± SEM from three independent experiments with >100 cells per each sample. Statistical significance was calculated by comparison to siControl#1 or siControl#2, using ordinary one-way ANOVAs with Tukey's test. *, $P < 0.05$; **, $P < 0.01$; ***, $P < 0.001$; ****, $P < 0.0001$.

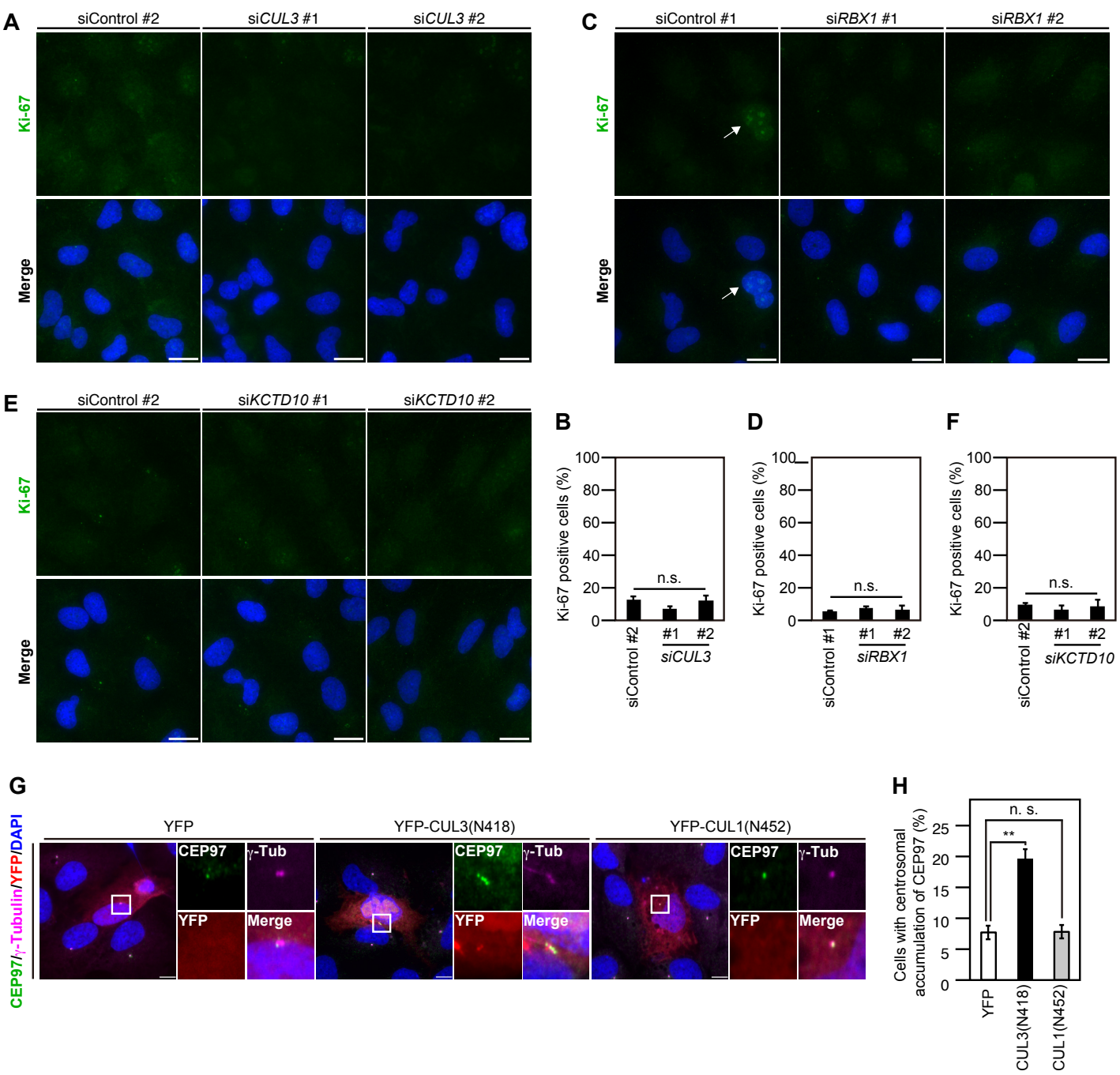

Fig. S4. Effects of *CUL3*, *RBX1* or *KCTD10* knockdown on serum starvation-induced cell quiescence and effects of overexpression of CUL3(N418) or CUL1(N452) on centrosomal localization of CEP97. causes centrosomal accumulation of CEP97. (A-F) Effects of knockdown on serum starvation-induced cell quiescence. RPE1 cells were transfected with siRNAs targeting *CUL3* (A), *RBX1* (C), or *KCTD10* (E), and serum-starved for 48 h. Cells were fixed and stained with an Alexa 488-conjugated anti-Ki-67 antibody (green) and DAPI (blue). Scale bar, 20 μm. The percentage of Ki-67-positive cells was quantified in *CUL3* (B), *RBX1* (D) and *KCTD10* (F) knockdown cells. Data are means ± SEM from three independent experiments with >200 cells per each sample. An arrow indicates Ki-67-positive nucleus. Statistical significance was calculated using ordinary one-way ANOVAs with Tukey' s test. n.s., not significant. (G) Effects of overexpression of CUL3(N418) or CUL1(N452) on centrosomal localization of CEP97. RPE1 cells were transfected with YFP, YFP-CUL3(N418), or YFP-CUL1 (N452) and serum-starved for 48 h. Cells were fixed and stained with anti-CEP97 (green) and anti-γ-tubulin (magenta) antibodies and DAPI (blue). Cells were also imaged by YFP fluorescence (red). Scale bar, 20 μm. Right panels show magnified images of the white boxes. An arrow indicates the centrosomal localization of YFP-CUL3(N418) (H) Quantification of the percentage of cells with centrosomal accumulation of CEP97. Data are presented as the mean ± SEM from three independent experiments with >50 cells per each experiment. Statistical significance was calculated using ordinary one-way ANOVAs with Tukey's test. n.s., not significant; **, $P < 0.01$.

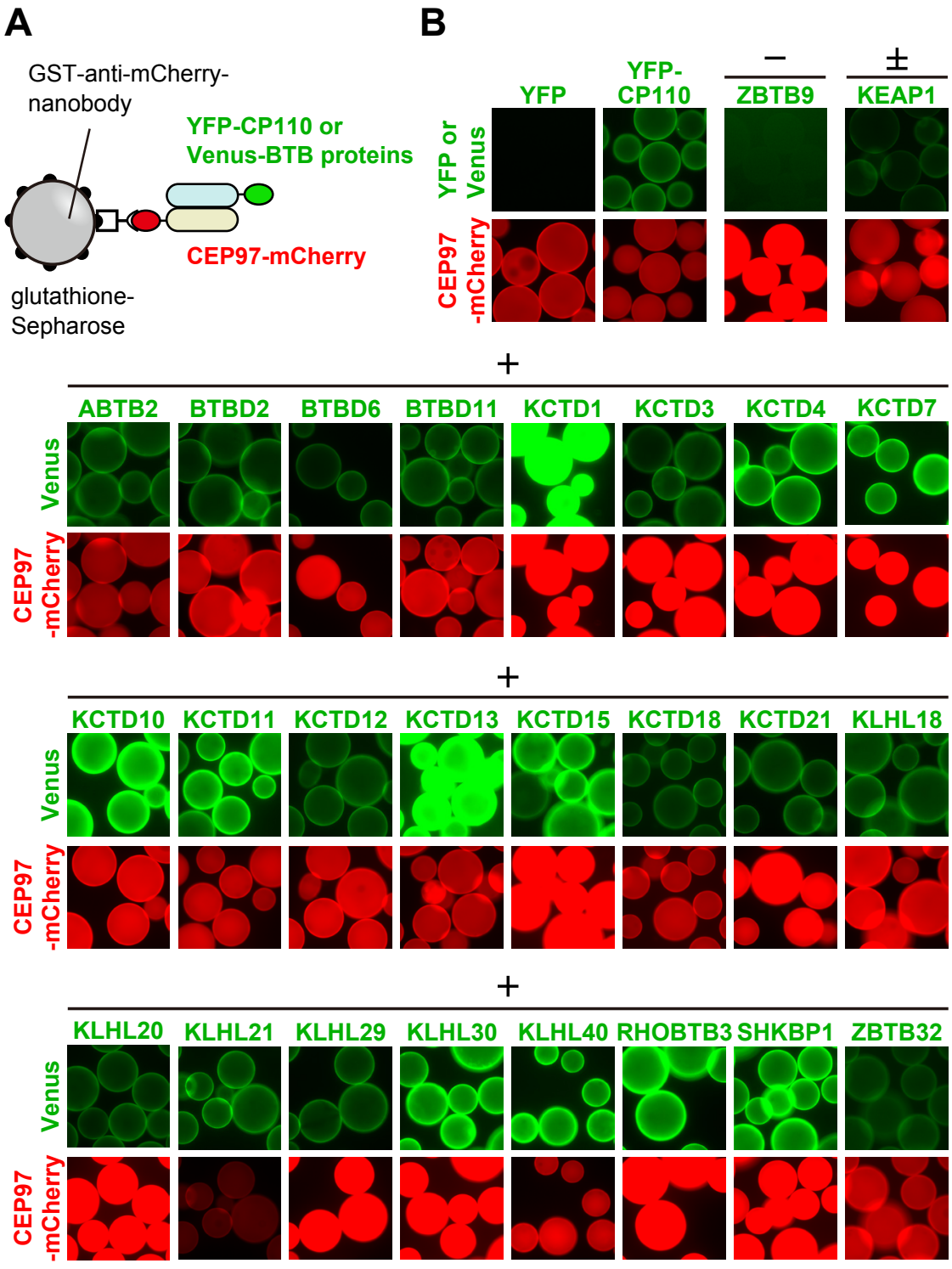

Fig. S5. Screening of BTB-containing proteins that bind to CEP97 by visible immunoprecipitation (VIP) assays. (A) Schematic diagram of the VIP assay. (B) Screening of BTB-containing proteins. HEK293T cells were co-transfected with CEP97-mCherry and YFP, YFP-CP110, or Venus-tagged BTB-containing proteins. Cell lysates were precipitated with a GST-tagged anti-mCherry nanobody pre-bound to glutathione-Sepharose beads. Beads were imaged by YFP or Venus (green) and mCherry (red) fluorescence. YFP and YFP-CP110 were co-transfected with CEP97-mCherry as negative and positive control, respectively. Results of VIP assays are shown on the top of the fluorescence images. +, intense signal; ±, weak signal (KEAP1); −, no or very weak signal (YFP and ZBTB9). Experiments were repeated three times and the results were reproduced in three independent experiments.

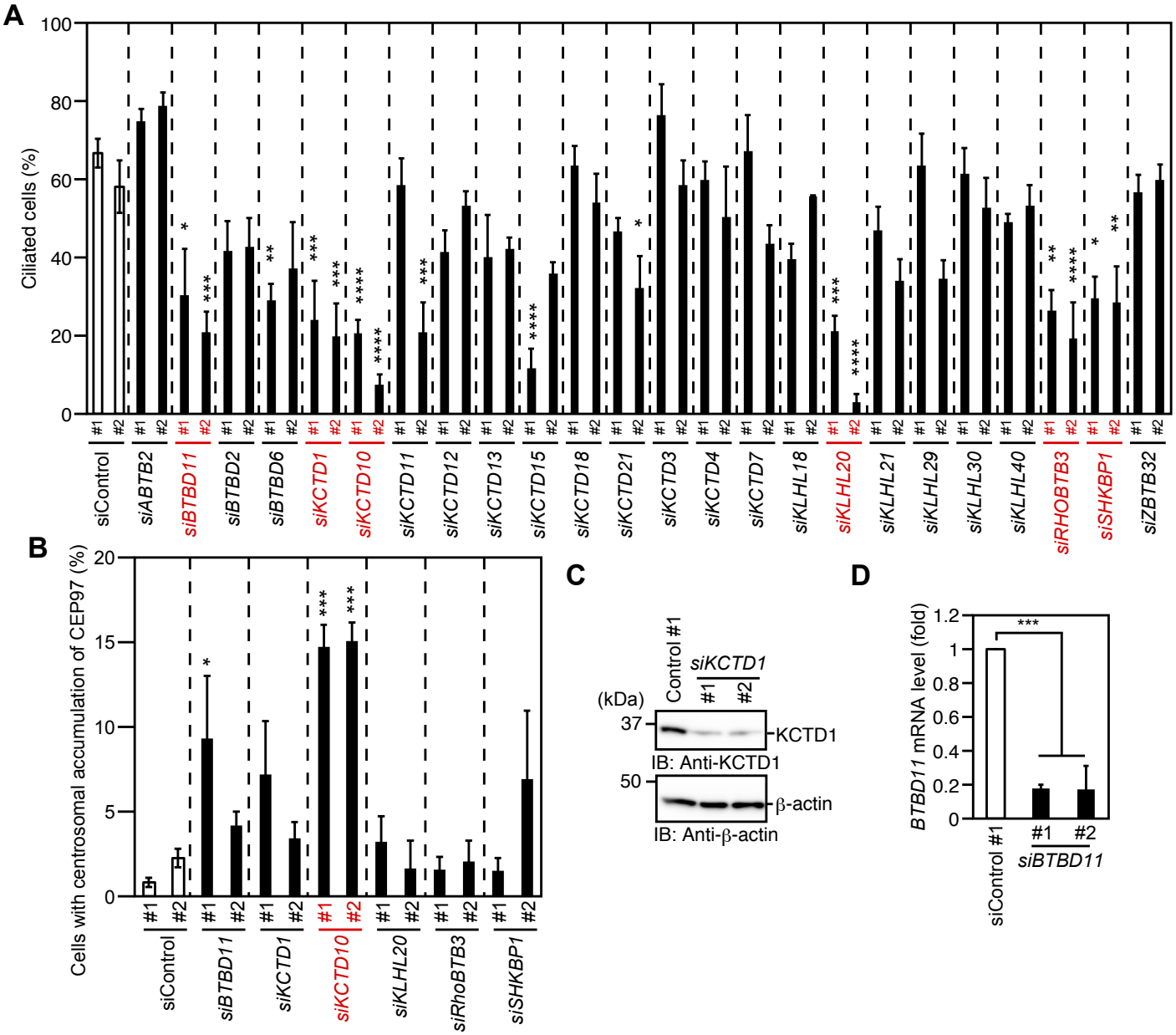

Fig. S6. Screening of BTB-containing proteins that are involved in CEP97 degradation and ciliogenesis. (A) Effects of knockdown of BTB-containing proteins in serum-starvation-induced ciliogenesis. RPE1 cells were transfected with two independent siRNAs targeting genes coding for indicated BTB-containing proteins. Cells were serum-starved for 48 h and then fixed. A graph shows the percentage of ciliated cells. Data are means ± SEM from more than three independent experiments with >100 cells per each sample. Statistical significance was calculated by comparison to siControl#1 or siControl#2. Genes for BTB-containing proteins indicated in red were selected as positive hits. (B) Effects of knockdown of BTB-containing proteins on the centrosomal localization of CEP97. RPE1 cells were transfected, cultured and then fixed as in (A). A graph shows the frequency of cells with aberrant accumulation of CEP97 on the centrosome. Data are means ± SEM from more than three independent experiments with >100 cells per each experiment. Statistical significance was obtained by comparison to siControl#1 or siControl#2. Statistical significance was calculated using ordinary one-way ANOVAs with Tukey' s test. *, $P < 0.05$; **, $P < 0.01$; ***, $P < 0.001$; ****, $P < 0.0001$. No asterisk on the bar indicates to be not significant to control. (C) Knockdown efficiency of *KCTD1* siRNAs. RPE1 cells were transfected with control or *KCTD1* siRNAs and cultured for 48 h. Cell lysates were analyzed by immunoblotting with anti-KCTD1 and anti-β-actin antibodies. (D) Knockdown efficiency of *BTBD11* siRNAs. RPE1 cells were transfected with control or *BTBD11* siRNAs and cultured for 48 h. Total RNAs were isolated and subjected to real-time quantitative PCR. Fold changes are normalized to control siRNA-transfected cells. Data are means ± SEM from three independent experiments. Statistical significance was calculated using ordinary one-way ANOVAs with Tukey's test. ***, $P < 0.001$

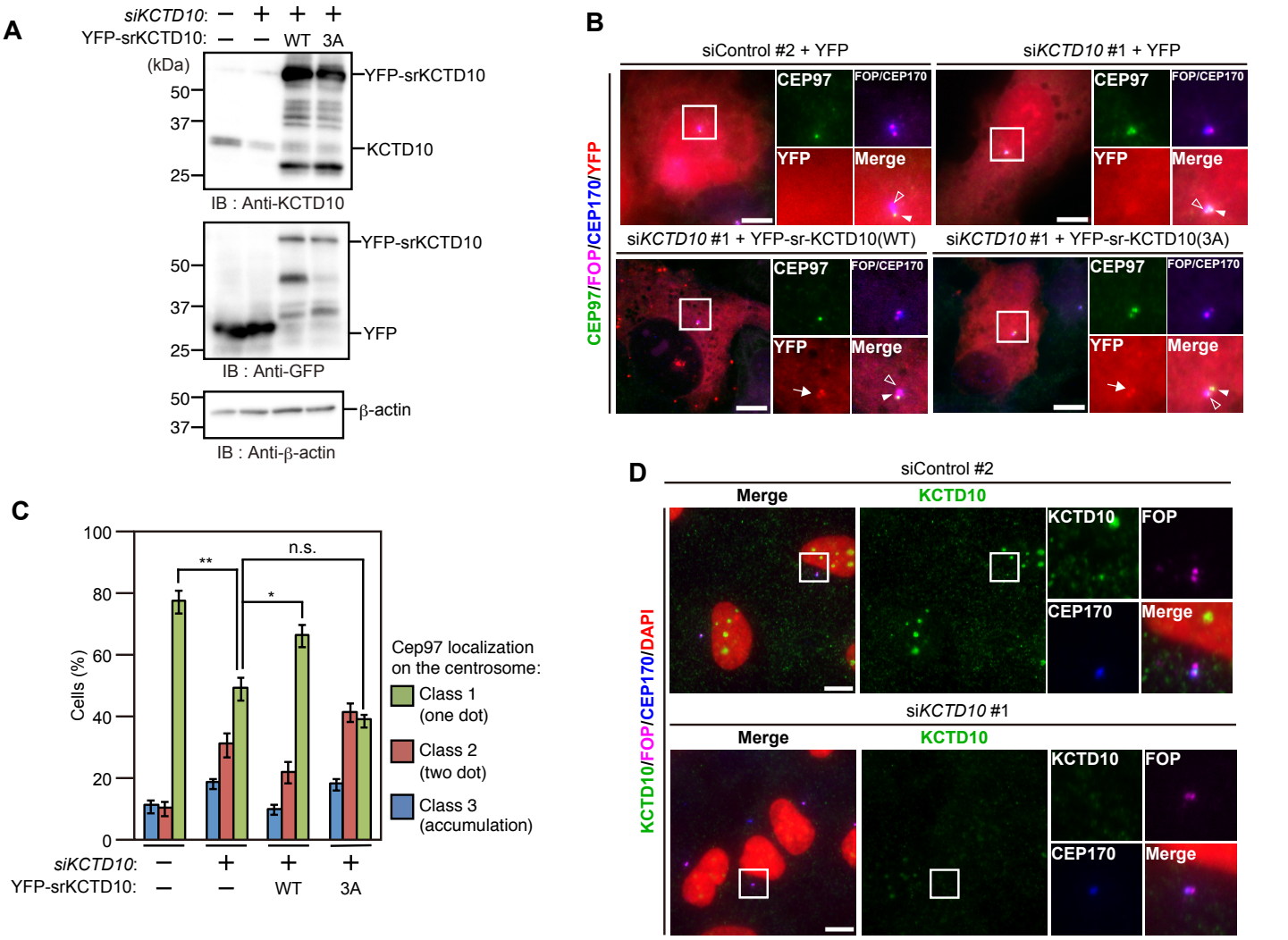

Fig. S7. Knockdown-rescue experiments for the effect of *KCTD10* siRNA on CEP97 localization on the centrosome. (A) Immunoblot analysis of the expression of YFP-tagged siRNA-resistant (sr)-KCTD10. RPE1 cells were co-transfected with control or *KCTD10* siRNA #1 and YFP or YFP-sr-KCTD10 (WT or 3A) and cultured for 72 h. Cell lysates were immunoblotted with anti-KCTD10, anti-GFP and anti-β-actin antibodies. (B) Effects of expression of YFP-sr-KCTD10 (WT or 3A) on CEP97 localization on the centrosome in KCTD10 knockdown cells. RPE1 cells were transfected as in (A), cultured for 24 h and then serum-starved for 48 h. Cells were fixed and stained with anti-CEP97 (green), anti-FOP (magenta) and anti-CEP170 (blue) antibodies. Cells were also imaged by YFP fluorescence (red). Scale bar, 10 µm. Right panels show magnified images of the white boxes. Arrows indicate the centrosomal localization of YFP-fused proteins. Outlined and white arrowheads indicate CEP170-bearing mother centrioles and daughter centrioles, respectively. (C) Quantification of the percentage of cells with CEP97 localization on one dot (green), two dots (red), or aberrant accumulation on the centrosome (blue). Data are presented as the mean ± SEM from three independent experiments with >50 cells per each experiment. Statistical significance was calculated using ordinary one-way ANOVAs with Tukey's test. *, $P < 0.05$; **, $P < 0.01$. (D) Assessment of the specificity of anti-KCTD10 immunostaining. RPE1 cells were transfected with control or *KCTD10* siRNA and cultured in 0.2% serum-containing medium for 48 h. Cells were fixed and immunostained with anti-KCTD10 (green), anti-FOP (magenta) and anti-CEP170 (blue) antibodies. DNA was stained with DAPI (red). Scale bar, 10 µm. Right panels show magnified images of the white boxes.

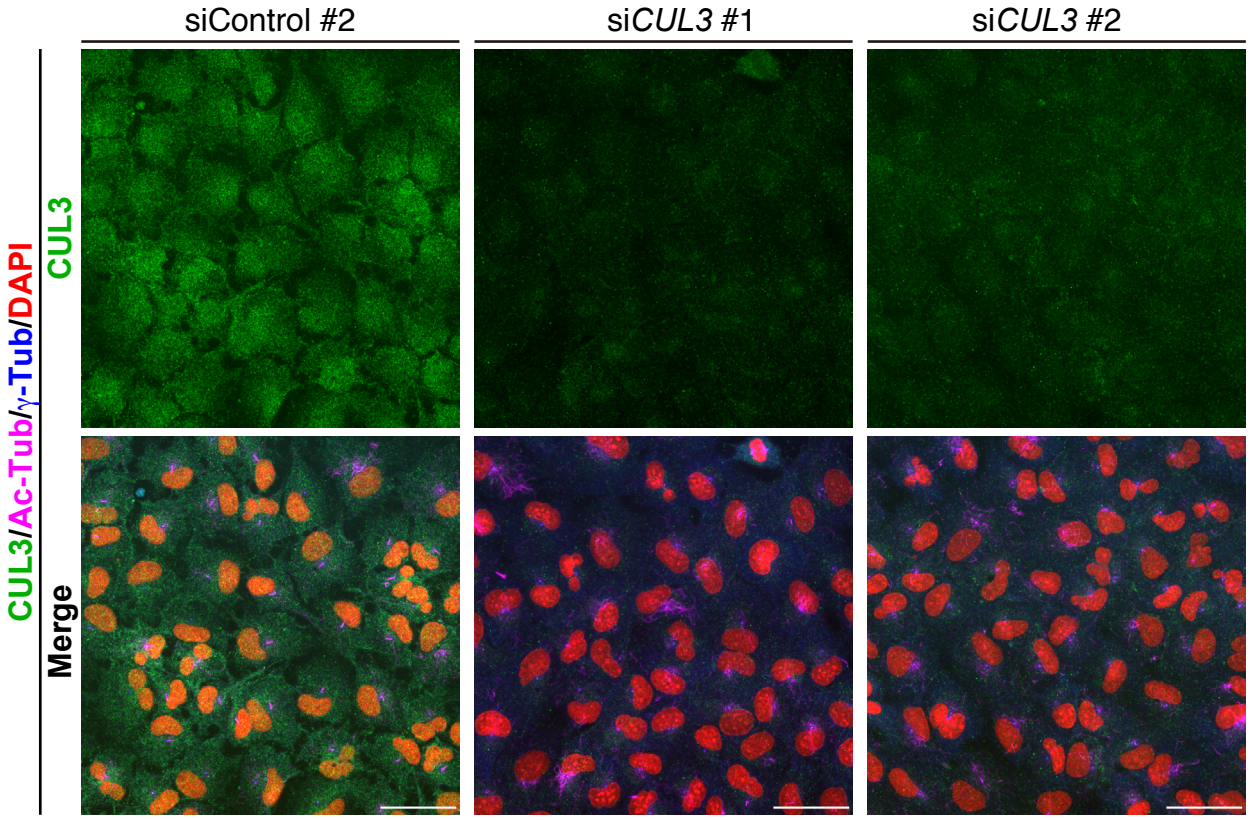

Fig. S8. Assessment of knockdown efficiency of CUL3 siRNAs by immunostaining. RPE1 cells were transfected with *CUL3* siRNAs and serum-starved for 48 h. Cells were fixed and stained with anti-CUL3 (green), anti-Ac-tubulin (magenta) and anti-γ-tubulin (blue) antibodies. DNA was stained with DAPI (red). Low power field image shows that knockdown of *CUL3* grossly reduced the intensity of anti-CUL3 immunostaining in most cells in the visual field.

Table S1. List of HuPEX clones used in this study.

Click here to Download Table S1

Table S2. List of HuPEX clones selected for VIP assay and their results.
Results of VIP assays are indicated as three symbols: +, intense signal; ±, weak signal; –, no or very weak signal.

Click here to Download Table S2

Table S3. List of antibodies used in this study.

Click here to Download Table S3

Table S4. List of siRNAs used in this study.

Click here to Download Table S4

Table S5. List of primers for PCR used in this study.

Gene name	Forward primer (5' → 3')	Reverse primer (5' → 3')
BTBD11	CAAAGCACTCCTCTCCAGCA	AATGAGCAGTGACTCTGGGC
UBC	ATTTGGGTCGCGGTTCTTG	TGCCTTGACATTCTCGATGGT